electronics

MDPI

Article

Magnetic Localization of Wireless Ingestible Capsules Using a Belt-Shaped Array Transmitter

Ivan Castro [1], Jan Willem de Wit [2], Jasper van Vooren [1], Tom Van Quaethem [1], Weixi Huang [1] and Tom Torfs [1,*]

1. IMEC Belgium, Kapeldreef 75, 3001 Leuven, Belgium
2. IMEC within OnePlanet Research Center, Bronland 10, 6708 WH Wageningen, The Netherlands
* Correspondence: tom.torfs@imec.be

Abstract: In the last 20 years, research into and clinical use of wireless ingestible capsules (WIC) has increased, with capsule endoscopy being the most common application in clinical practice. Additionally, there has been an increased research interest in sensing capsules. To maximize the usefulness of the information provided by these devices, it is crucial to know their location within the gastrointestinal tract. The main WIC localization methods in research include radio frequency approaches, video-based methods, and magnetic-based methods. Of these methods, the magnetic-based methods show the most potential in terms of localization accuracy. However, the need for an external transmitting (or sensing) array poses an important limitation, as evidenced by most of the reported methods involving a rigid structure. This poses a challenge to its wearability and performance in daily life environments. This paper provides an overview of the state of the art on magnetic-based localization for WIC, followed by a proof of concept of a system that aims to solve the wearability challenges. Comparative performance simulations of different transmitter arrays are presented. The effect of including one or two receiver coils in the WIC is also evaluated in the simulation. Experimental localization results for a planar transmitter array and for a more wearable belt-shaped transmitter are presented and compared. A localization mean absolute error (MAE) as low as 6.5 mm was achieved for the planar array in a volume of 15 cm × 15 cm × 15 cm, starting at a 5 cm distance from the transmitter. Evaluating the belt array in a similar volume of interest (15 cm × 15 cm × 15 cm starting at 7.5 cm distance from the transmitter) resulted in an MAE of 13.1 mm across the volume and a plane-specific MAE as low as 9.5 mm when evaluated at a 12.5 cm distance. These initial results demonstrate comparable performances between these two transmitters, while the belt array has the potential to enable measurements in daily-life environments. Despite these promising results, it was identified that an improvement in the model for the magnetic field when using transmitter coils with ferrite cores is necessary and is likely to result in better localization accuracy. This belt-array approach, together with compensation techniques for body motion, as recently reported for rigid arrays, has the potential to enable WIC localization in uncontrolled environments with minimal impact on the user's daily life.

Keywords: wireless ingestible capsule; sensing capsule; magnetic localization; wearable transmitter array

1. Introduction

Localization of wireless ingestible capsules (WIC) is a research topic that has gained interest in the last decade due to the increased research into and clinical use of WICs. Since the commercial release of the first WIC in the form of a capsule endoscope (CE) by Given Imaging (Now PillCam by Medtronic [1]) in 2001, other WICs have been the focus of research and have been introduced to the market. Currently, several commercial CE devices are available, including PillCam by Medtronic [1], Endocapsule by Olympus [2], Capso-Cam by CapsoVision [3], MiroCam by IntroMedic [4] and Omom by Jinshan Group [5]. These CEs focus on imaging of the gastrointestinal (GI) tract, although some variations

include other functionalities for specific diseases (e.g., SmartPill Motility Testing System by Medtronic [6]).

In addition to commercially available WICs, several investigational devices and proof-of-concept prototypes have been reported in the literature. These devices include additional functionalities that aim to aid in the diagnosis of numerous GI-related conditions. Besides measurement of pH and temperature, some of these additional functionalities include the capability of measuring gases within the GI tract (O_2, H_2, CO_2) [7], performing electrochemical sensing [8], infrared fluorescence [9], drug delivery [10], bio-molecular detection [11] and sampling of the gut microbiome [12], among others. An overview of emerging technologies in the WIC field and the upcoming challenges is summarized in [13–15].

Accurate localization of WIC devices has thus become increasingly important, as these are evolving from image acquisition devices into multi-modal sensor units with the potential to play an important role in the diagnosis of multiple GI-related diseases. It is therefore crucial to include information on the location of specific measurements within the GI tract in the acquired data. This will enable better identification of the physiological location of GI abnormalities, maximize the usefulness of the collected data and facilitate location-dependent actions such as drug delivery and sampling.

Different techniques have been researched over the last decade for WIC localization, with radio frequency (RF) techniques being the most common and used in some commercial CEs. However, RF-based techniques have drawbacks related to the penetration depth and inhomogeneities within the human body. Other techniques based on computer vision and magnetic fields have thus been the focus of research, as they have important advantages due to the homogeneous permittivity of the human body to (static and quasi-static) magnetic fields and promising results in terms of spatial accuracy.

A limitation identified in the magnetic-based methods reported in literature is the wearability of the proposed solutions. While small localization errors have been reported in evaluations of magnetic-based solutions, they tend to require an external array of sensors or coils that are comprised of rigid structures and are thus considered impractical for wearable systems [16].

This work aims to evaluate a proof of concept of a system that would increase the wearability of the required external transmitter when performing magnetic-based localization. To this end, comparative performance simulations were conducted for different transmitter arrays that would improve the wearability of such systems. Based on these simulations, the selection to build a belt-shaped array transmitter was made, which was then evaluated and compared against measurements from a planar array.

2. State of the Art

The most researched WIC localization methods are radio frequency (RF)-based methods, video-based (computer vision) methods and magnetic and electromagnetic-based methods. Other less researched methods include ultrasound, the use of inertial measurement units (IMUs) and in-hospital techniques such as X-ray imaging and magnetic resonance imaging (MRI), which are commonly used as a ground truth when evaluating methods in the above-mentioned categories, but require bulky equipment that does not allow for a portable system.

RF-based methods include localization techniques that use the received signal strength (RSS), the time of flight (ToF), direction of arrival (DoA) and radiofrequency identification (RF-ID). One advantage of RF methods is that the in-pill hardware used for communication (typically at frequencies in the range of a few hundred MHz) is also used for RF-based localization. This is an important benefit given the space and power restrictions of WIC devices. However, the localization accuracy and general performance of these methods is significantly affected by the non-homogeneous attenuation of RF signals within the human body.

Overall, localization errors reported for received signal strength indicator (RSSI) techniques are typically in the order of 40 mm [17,18] to 80 mm [19]. Most of these RF-based

approaches try to compensate for the in-body non-homogeneous signal absorption in some way. This involves using human body models or averaged attenuation estimations [20–22]. Some efforts to perform RSS-based localization without prior knowledge of body characteristics or antenna properties have been reported, with simulated root mean square error (RMSE) results ranging from 35 mm to 36 mm [23]. It is worth noting that most of the available literature is a result of simulations, and the few reported experimental results include either homogeneous phantoms [24] (error of 20 mm) in vivo measurements with restrictions, such as antenna alignment and a maximum distance between external antenna and WIC of 80 mm [25] (error of 10 mm based on two measurement points).

Because of its relatively simple implementation and the advantages of already having an in-pill RF source for communication purposes, RSSI has been the method included in some of the commercially available pills that offer localization capabilities. The most well-known examples of this are the PillCam by Medtronic [1] (Previously Given Imaging), and the Olympus Endocapsule 10 [2]. The former includes a set of eight sensors attached to the abdomen and chest. This system provides a two-dimensional localization and has been characterized using in vivo experiments to achieve a mean absolute error (MAE) of 37.7 mm and a maximum error higher than 100 mm [26]. This level of accuracy and the limitation to two-dimensional data may be useful for a rough indication of the location of CEs but is likely insufficient when used within the emerging WICs, which have an increased number of sensors and aim to diagnose and treat a high number location-dependent GI conditions.

In the case of the Olympus Endocapsule, a three-dimensional localization method is used, which also uses a set of seven to eight patch antennas in combination with two external units. This system was evaluated in vivo, with individual axis errors ranging between 20 mm and 25 mm, and propagated errors between 53.2 mm and 73.9 mm [27]. It is worth noting that, in this study, it was found that the total spatial error and the body mass index (BMI) of the volunteers were correlated, which highlights a limitation of RSSI-based methods.

The more complex ToF and DoA techniques have also been primarily evaluated in simulation environments, with lower errors than RSSI methods being reported. This includes ToF averaged errors ranging from 8.8 mm [28] to 15 mm [17,29]. Simultaneous ToF and DoA with IMU data methods were reported to achieve errors below 10 mm when integrated into a Kalman filter approach [30]. Similar results have been reported for standalone DoA techniques [31]. In an attempt to avoid the use of an a-priori average permittivity in ToF methods to estimate propagation velocity, as done in [17,29] other authors have reported an RSS-based estimation of this parameter, resulting in an error of approximately 2 mm when combined with a ToF technique [32]. However, most research in this field is based on simulations and relies on the use of human body models. This makes it less likely to maintain the simulated performance in real-life environments, where the position of the different organs and body structures changes between different individuals and over time within the same individual.

The use of RF-ID tags has also been explored for localization purposes, although these are less common in the literature [33]. In [34], a method using RF-ID and a cubic antenna array was reported, resulting in errors below 7.8 mm when tested in air. An example of such a passive RF-ID localization method is found in the commercial device Calypso by Varian Medical System Inc., which reports accuracies of 2 mm using a clinical tabletop device [35] and is reported to be limited to a depth of 16 mm to 20 mm [36]. Similar approaches using LC markers have been reported in [37,38]. For a more detailed analysis of RF-based methods, the reader is referred to [16,20,39].

Since CE devices already capture images of the GI tract, another explored method is the use of these images together with computer vision techniques in order to perform a rough identification of the different parts of the GI tract, or even compute their relative displacement based on consecutive images [16]. The PillCam by Medtronic already makes use of some of its images to perform an identification of entrance to the stomach, passage in the pylorus and passage through ileocecal valve [26], which is then used to estimate GI

transit times. Other more elaborate camera-based methods have been reported [40–43], but these still need to be evaluated in more realistic conditions [16].

A category of techniques that is currently gaining attention uses DC and low-frequency (also termed quasi-static) magnetic fields, overcoming limitations of the RF-based techniques regarding body inhomogeneities. These take advantage of the homogeneous permeability of the human body to these fields, which is almost equivalent to that of air. The 'quasi-static' electromagnetic region is defined as the region significantly smaller than one wavelength [44], in which it can be assumed that the magnetic and electric fields are decoupled. The WIC localization magnetic-based techniques can vary depending on whether the magnetic field is generated externally (i.e., outside the body) or internally (i.e., within the WIC). For externally generated fields, these fields can be DC fields creating a characteristic field gradient or AC fields from which the amplitude can typically be modelled as a function of the measurement location and orientation. Internally generated fields can be achieved by either permanent magnets or by electromagnets. Figure 1 provides an overview of the mentioned magnetic-based approaches.
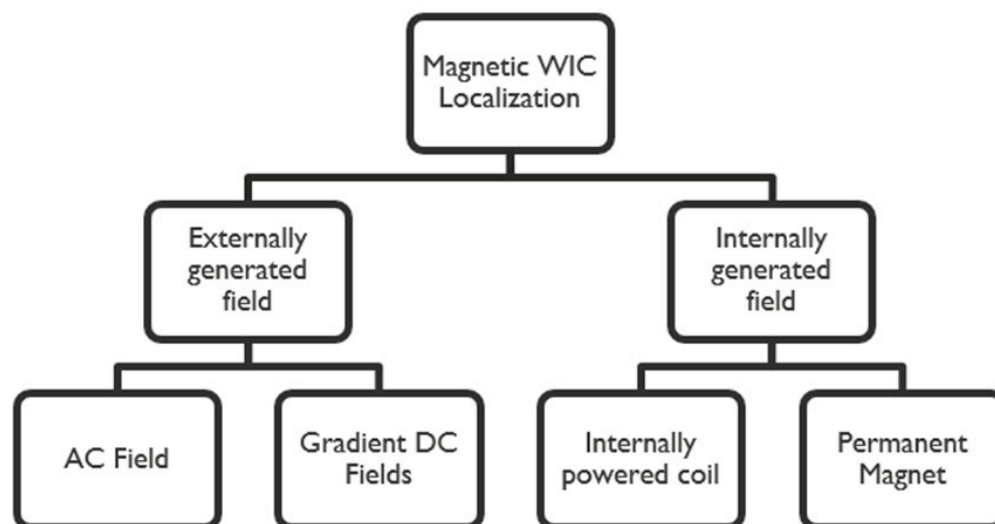

Figure 1. Overview of the most commonly researched magnetic-based WIC localization methods.

One of the most common approaches reported when magnetic-based localization of WICs started was the use of a permanent magnet. In this method, a magnet is included within the WIC, and the DC magnetic field caused by it is measured using an external sensor array. The Magnetic Tracking System MTS-1, was one such system developed by the Swiss company Motilis Medica. It used a planar array of Hall-effect sensors [45] to evaluate GI motility and was able to perform magnet tracking up to a distance of 20 cm from the sensor array. In vivo evaluations of this system in controlled (non-ambulatory) conditions showed its ability to provide useful data related to gastrointestinal transit times and motility [46–48]. The results showed an agreement between estimated trajectories and reference radiographic images [49].

The same company later reported an update to the system by switching to a AC magnetic fields [50] to overcome the need for a controlled environment when using DC fields from a permanent magnet. These fields are of the same magnitude as the earth's magnetic field and have a significant impact on the system's calibration [51]. For this purpose, the in-pill magnet was replaced with an electromagnet, and the signals were measured using four sensors placed in a receiver plate on the abdomen, as shown in Figure 2. Although no spatial localization errors were reported, physiological validation showed region-specific contraction patterns and helped in the computation of the transit times, which agreed with the times calculated based on radio opaque markers. It is worth noting that for motility-oriented pills, the complete pill volume is dedicated to the

localization/motility functionality. This is not possible in other WICs such as CE or multi-sensor WICs where the space available for localization-related components is significantly reduced. In an effort to reduce the space occupied by the localization components, a WIC with an ASIC was also presented by the company [52,53], which allowed the pill diameter to be reduced from 8 mm to 6 mm.

Figure 2. WIC, sensor array and receiver system presented by Motilis Medica when moving to an AC magnetic localization method [50] from their previous approach of using a permanent magnet within the WIC.

Similar to the initial system reported by Motilis Medica based on an in-pill permanent magnet, other systems have been reported together with experiments evaluating the spatial localization accuracy of such a method. Typically, these methods make use of the dipole model and optimization algorithms to estimate the location of the magnet. In [54], a magnet with a diameter of 6 mm and a length of 12 mm was shown together with a planar 4-sensor array and a calibration method for system orientation, resulting in an error of 5 mm when evaluated in a volume of 20 cm × 20 cm × 20 cm. The system was also tested in vivo, and locations were visually compared against X-ray images. Similar results (MAE of 5.6 mm) were achieved by using a planar array of 16 Hall-effect sensors [55].

With the purpose of increasing the localization volume and improving the accuracy, researchers have also reported three-dimensional sensor arrays for the localization of permanent magnets. Examples include a cubic array (Figure 3a) of $0.5 \times 0.5 \times 0.5$ m^3 with 16 sensors per side of the cube that resulted in an average error of 1.8 mm [56] as well as a cylinder-like array with 32 sensors (Figure 3b) that resulted in a 3.82 mm error [57] when applying compensation algorithms based on two external magnets.
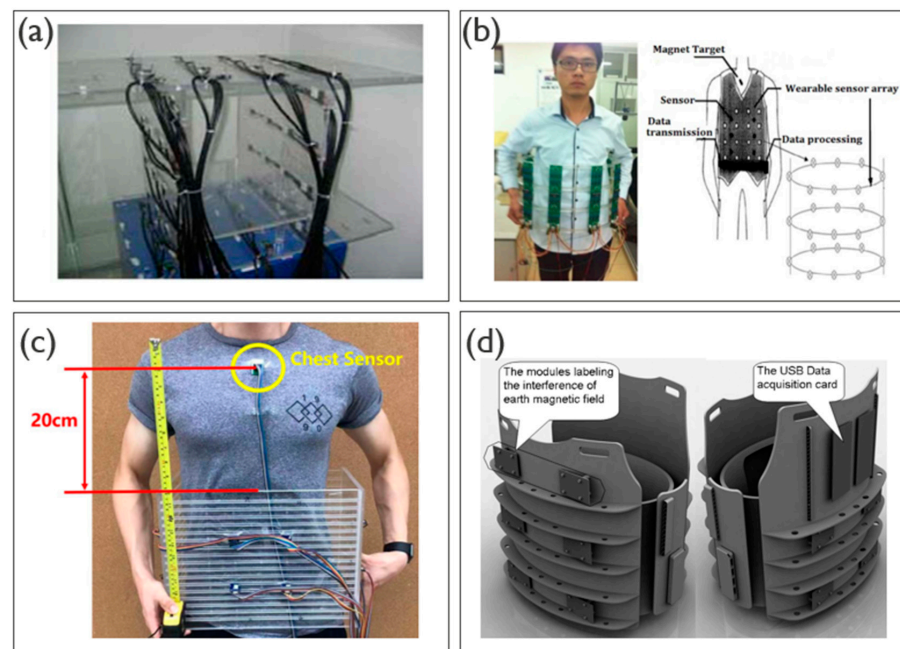
Figure 3. Examples of three-dimensional sensor arrays proposed in literature for WIC localization based on an in-WIC permanent magnet. (**a**) $0.5 \times 0.5 \times 0.5$ m^3 cubic array with 16 magnetic sensors per face proposed in [56]; (**b**) cylinder-like array with 32 sensors proposed in [57], including a compensation algorithm based on two external magnets; (**c**) sensor array proposed in [58] together with additional magnetic sensors on the surface of the body for motion compensation; (**d**) sensor array proposed in [59] with geomagnetic field compensation.

Because of the known interference from the Earth's magnetic field and the sensitivity to changes in orientation, compensation algorithms have been reported, ranging from static algorithms that assume a fixed orientation of the sensor array with respect to Earth's magnetic field [54] to methods that use additional sensors such as IMUs, allowing for an error of 4 mm [60]. Other systems include additional magnetic sensors on the surface of the body (Figure 3c) resulting in a 10 mm error [58] and methods for two-dimensional localization without using additional sensors for compensation with errors of 3 mm [61] and 8 mm [62].

It is clear from the state of the art of using permanent magnets for WIC localization that these systems have the potential to achieve mm-level accuracy. Nevertheless, the fact that a planar array is not sufficient to achieve localization that covers the complete GI tract [16] and that three-dimensional sensor array structures such as the ones shown in Figure 3 are necessary makes this solution less attractive for an ambulatory environment. In addition, the inclusion of a magnet within the WIC significantly reduces the available space for other required components such as battery, sensors and required electronic circuitry. Specially taking into account that the size of the magnet plays an important role in the localization errors and that most of the reported research using DC fields uses magnets with dimensions on the order of 1 cm (12 mm $\times$ 6 mm [54], 10 mm $\times$ 10 mm [60,61] 15 mm $\times$ 10 mm [58,62], 5 mm $\times$ 10 mm [63], 5 mm $\times$ 3 mm [59]). Smaller magnets imply the need for a bigger sensor array (Figure 3d) [59] to compensate for the lower magnetic field. Furthermore, only one WIC can be used at a time, and a permanent magnet in the WIC poses additional safety risks. For example, it will not be possible to undergo an MRI scan in the case of an emergency.

Few approaches using DC magnetic fields generated from outside the body have been reported [64,65]. These approaches use the principle of magnetic gradient present in MRI devices but require a relatively high field to avoid disturbances from the earth's magnetic field. In [65], a WIC was presented with a gradient-based localization system that achieved

a mean resolution of 1.5 mm. However, this system required a set of transmitting coils that needed 15 A of current (800 W) and weighed 18 Kg. An alternative system was discussed that would require 350 mA of current with a weight of 1.2 Kg, and had the potential to achieve a mean resolution of 7.5 mm. In vivo animal validation was presented using two sets of the 15 A gradient coils with errors between 0.54 mm and 6 mm, demonstrating the feasibility of the concept when used in human bodies. Nevertheless, the wearability of the system is rather limited, even when considering the alternative transmitter proposed.

The use of quasi-static (i.e., low frequency) magnetic fields has been presented as a technique that has several advantages over RF-based methods and the use of in-WIC permanent magnets. While in some cases, the AC magnetic field is generated from within an electromagnet in the pill [50], most of the research has focused on the external (out of body) generation of magnetic fields and the internal (inside the WIC) sensing of these fields. This is likely due to the power requirements of generating the field within the WIC and the tradeoff it implies regarding the available power for other sensing functionalities.

Solutions that use an external AC magnetic field employ the same working principle as commercially available systems in the fields of tracking of surgical instruments (Aurora system by Northern Digital Inc. -103 Randall Drive. Ontario, Canada-) [66] and other applications such as sports tracking (Pholemus Inc. -40 Hercules Dr. Colchester, VT, USA-) [67] and VR systems (AmfiTrack by Amfitech. -Jens Grøns Vej 2. Vejle, Denmark- [68]). This method has the advantage of being immune to DC magnetic field variations with changing orientation and hence does not need geomagnetic compensation.

One of the earliest works that reported this approach for miniature receiving coils [69] (and hence with the potential to be integrated within a WIC) showed sub-mm errors by using a 3 mm × 0.9 mm sensing coil and an 8 × 8 planar array of transmitting coils (Figure 4a). This method was used for an initial position estimation followed by the use of an 8-coil subarray for position tracking. In this case, a current of 1 A at 50 kHz was used in the transmitter. The algorithm included a dipole model for the source and a Levenberg-Marquardt optimization algorithm to obtain the estimated location. A localization range of 200 mm above the planar array was reported. This concept was further evaluated by the authors in eye-tracking applications in animals [70] and humans [71].
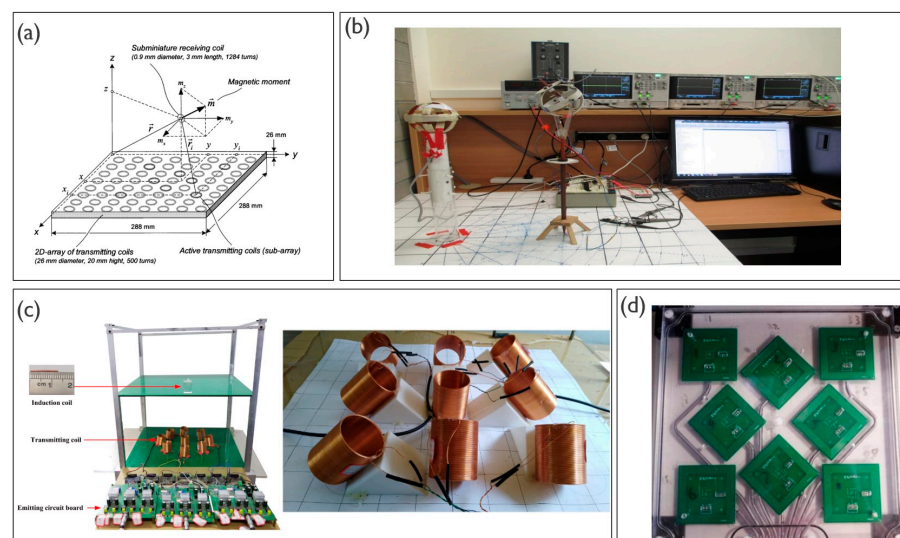

Figure 4. Example of systems for magnetic-based localization. (**a**) One of the earliest works reporting magnetic-based localization for miniature receiving coils using an 8 × 8 planar transmitter array [69]; (**b**) magnetic-based localization reported for WIC localization application with three-dimensional pill-shaped receiving coils and a 9.5 cm transmitting sphere [72]; (**c**) WIC localization approach with a one-dimensional receiver and an array of 9 transmitting coils [73]; (**d**) magnetic-based localization system with a planar array of 8 transmitting coils for virtual bronchoscopy applications [74].

An application for WIC localization was reported in [72]. Three sensing coils wound in a pill-shaped structure were used as sensing unit, and a set of three orthogonal coils in a sphere with a diameter of 9.5 cm (Figure 4b) and a current of 0.6 A (7.7 kHz) were used as the transmitting array. When tested in two positions, errors between 2.4 mm and 12 mm were reported for individual axes. Additional research by the authors [75] presented a system in which both the transmitting and receiving coils were configured in resonance, in order to increase the efficiency of the transmitter and the gain of the sensing coil. In this case, errors below 3 mm were achieved for a distance up to 200 mm from the transmitter sphere. A similar approach using a one-dimensional coil around the pill was presented in [76], without details on the characteristics of the field generator.

Similarly, an array of nine coils (Figure 4c) was used simultaneously at different frequencies (0.2 to 1.8 kHz) and with a driving current of 3 A, as presented in [73], together with a one-dimensional receiver coil of 12.7 mm $\times$ 0.8 mm. Errors of 2.3 mm were reported in a range of 500 mm when the receiver coil was aligned with the transmitting coils. Other magnetic-based localization systems for applications different than WIC localization have been reported in the literature [70,71,77,78], mostly using a planar transmitter array (Figure 4d) and at least one receiving coil.

An alternative to the use of sensing coils inside the WIC is to use a magnetic sensor with sufficient bandwidth to sense the magnetic field at the quasi-static frequency. This approach was presented in [79], where a magnetoresistive (MR) sensor was used in combination with a uniaxial transmitter coil operating at 2.5 kHz. The advantage of using such sensors is that three-dimensional fields can be measured while occupying a smaller volume than typical receiver coils. Nevertheless, the sensitivity of such MR sensors is relatively low (1 mV/V/Gauss in this case) and dependent on the supply voltage, which is typically limited within a WIC system. This translates into just 18 μV/μT for a system with 1.8 V supply and 33 μV/μT for a 3.3 V system. This sensitivity is significantly lower than typical sensitivities of 0.1 V/Hz T (2.5 mV/μT at 25 kHz) reported for coil-based magnetic localization systems [80]. This specific work using an MR sensor reported an error of 2.6 mm for a distance below 200 mm between transmitter and sensor, but the transmitter current and the voltage supply used for the MR sensor were not specified.

Research on magnetic-based localization methods for WIC and other localization purposes has shown promise due to the mm-level accuracy they can provide, and the fact that the human body can be considered as "transparent" for DC and low-frequency magnetic fields. This helps to overcome the limitations of the common RF-based methods, where models and assumptions are necessary. Despite the need to include additional hardware in the WIC (at least a receiver coil and signal pre-processing circuitry) and the possible interference from nearby ferromagnetic materials (including some of the WIC components), magnetic-based localization of WIC (particularly the quasi-static approach) is expected to be an important component of upcoming investigational and commercial ingestible devices.

Despite these advantages and the elaborate prototypes that have been presented in the last decade, there is an important aspect on wearability that has not been adequately addressed. The prototypes shown in Figure 3, which use a permanent magnet, as well as those shown in Figure 4, which use low-frequency magnetic fields, rely on sensing (for the magnet approach) or transmitting (for the quasi-static approach) structures that have limited wearability. This presents an inconvenience when attempting to perform WIC localization while allowing the person to perform their daily life activities. Recent reviews agree that the main limitation of the magnetic field-based methods is the use of a rigid sensor/coil array, which is not practical for a wearable system [16]. Another aspect related to the wearability that should be considered is the power consumption of the system, including the batteries required for a wearable system and the self-heating of these external units.

Moreover, the relative motion of external devices with respect to the body can be a source of additional localization error. To correct for this, compensation algorithms have

been proposed. Complementary to these algorithms, an external unit that reduces motion with respect to the body will minimize the error caused by body movements. In general, an external unit (specifically, the transmitter unit in the quasi-static approach) with as few wearability limitations as possible for the user, and allowing ambulatory WIC localization, has yet to be presented. Therefore, this work presents a prototype that aims to bridge this gap and serve as the first step towards a wearable WIC localization system.

3. Materials and Methods

The goal of this work is to improve the wearability of a magnetic-based localization system. An existing system from the state of the art was selected as a starting point and basis for comparison. Therefore, one of the simulated and built systems followed the localization solution 'Anser EMT' [77,81]. Specifically, the planar transmitter (Figure 4d) reported in this system (aimed for tracking of virtual bronchoscopy systems [74]) as well as the use of a model based on the Biot-Savart law for square coils was used. This work also involved a MATLAB-based optimization solver that used a 'Trust Region' algorithm [82], which is considered an evolution of the commonly used Levenberg-Marquardt algorithm [45,55,70].

3.1. Wearable Transmitter Concepts and Simulations

As an initial step towards evaluating a more wearable alternative for a transmitter unit to be used within a low-frequency magnetic localization system for WICs, different wearable concepts were proposed, as shown in Figure 5. These include the use of a belt-worn 'box' comprised of multiple three-dimensional coils (Figure 5a), a belt with the same type of coils worn on the waist (Figure 5b), a chest belt similar in form factor to some fitness trackers, also populated with small coil cubes (Figure 5c) and patches on the skin distributed on the chest and abdominal area and/or on the subject's back (Figure 5d).
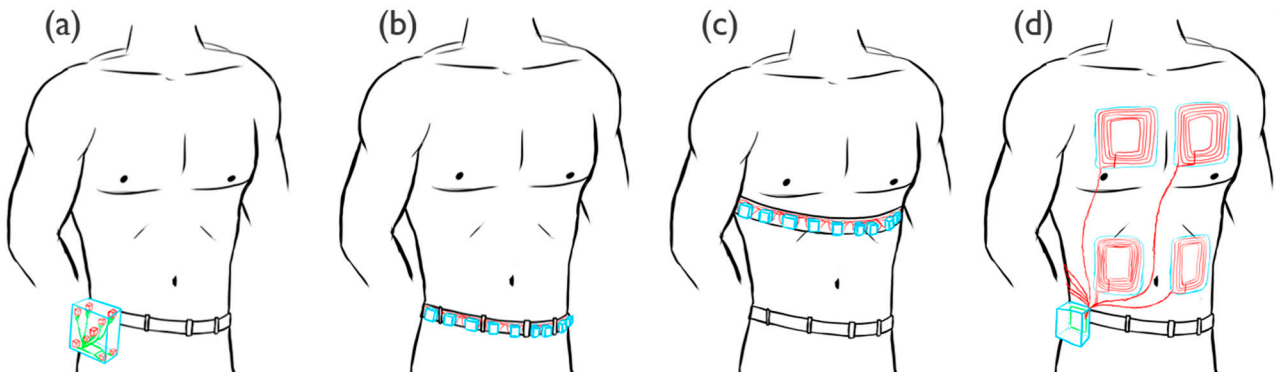

Figure 5. Proposed wearable transmitter concepts. (**a**) Box transmitter concept with transmitting coils in red; (**b**) waist-worn belt array concept with transmitting coils in blue; (**c**) chest-worn belt array concept with transmitting coils in blue; (**d**) skin patch array concept with transmitting patches and wiring in red.

These concepts were initially evaluated by simulating the magnetic field from each of the arrays. This was done using the Python library MagPyLib [83] to obtain the three-dimensional magnetic field in each points of a cube of dimensions of 20 cm × 20 cm × 20 cm, as shown in Figure 6 for the belt array. To emulate the use of a one-dimensional receiver, an arbitrary orientation of the receiver was selected (in this case $10°,15°$ in a spherical coordinate system). After this, the simulated values were used to perform the localization estimation with different levels of noise added to evaluate the robustness of each of the proposed arrays in the presence of noise. The specific variations in the simulations presented here include: an array of nine three-dimensional coil cubes for the box transmitter (Figure 5a), an array of 12 three-dimensional coil cubes for the belt transmitters (Figure 5b,c) and an array of eight planar coils for the patch array (Figure 5d). In the case of the belt simulation, only a waist configuration was simulated due to the symmetry of placing the belt in the waist or in the

lower chest with respect to the main area of interest, as shown in Figure 6a,b. Performance differences between these waist and chest belt concepts are only expected to be seen when evaluating the system under real-life conditions, where the waist location is expected to require more complex motion compensation algorithms due to the relative movement of the abdominal area with respect to a subject's waist.
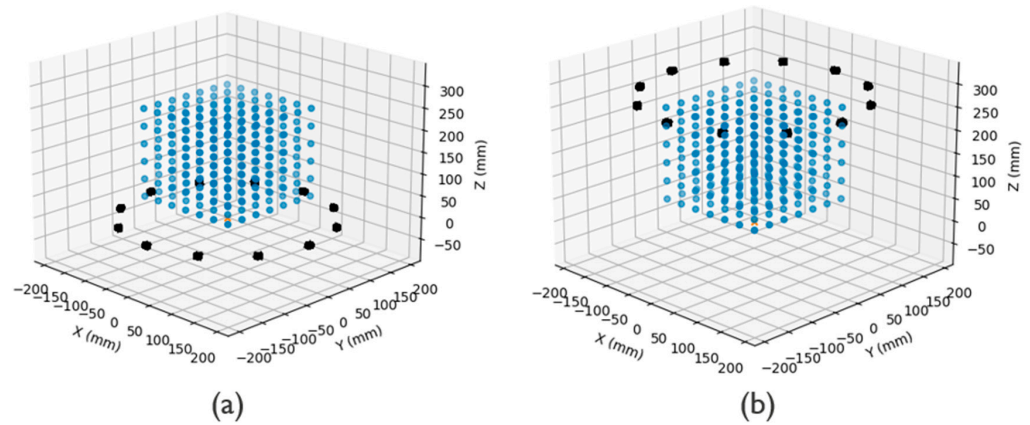

(a) (b)

Figure 6. Representation of the simulation datapoints used in the evaluation of the transmitter concepts. Belt transmitter is shown for reference. Equivalent symmetric simulation space for belt worn in waist (**a**) and worn in lower chest (**b**) is depicted. Due to the equivalence, a single belt simulation was conducted. Blue dots correspond to sampling points while black cubes correspond to transmitting 3D coils.

An additional simulation was conducted to compare having a one-dimensional receiver in the WIC to having two orthogonal receiver coils. In this simulation, the optimization algorithm was updated to receive input from two receiver coils and perform the localization estimation using three different approaches: (A) performing an independent localization estimation and obtaining the average location (Figure 7a); (B) providing both values as inputs to the least squares solver and thus doubling the number of values/equations within the objective function (Figure 7b); (C) calculating the resulting magnetic vector from both measurements and using it as an input for the location estimation algorithm (Figure 7c). Theoretically, it is expected that the second of these options would provide better results since the optimization algorithm has more information available.
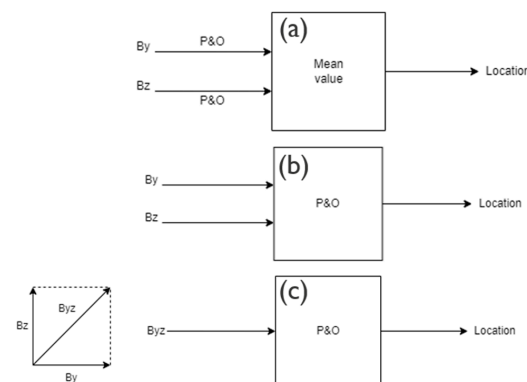

Figure 7. Graphical representation of the three position and orientation (P&O) algorithm implementations used for the simulations evaluating a two-dimensional receiver. (**a**) Independent localization estimation and average location; (**b**) two values as inputs to the least squares solver; (**c**) use of the resulting magnetic vector from both measurements.

3.2. System Architecture

As mentioned above, the goal was to implement a reference transmitter (the planar array from Figure 4d) and one of the proposed wearable transmitter arrays for comparison purposes. Based on the simulation results (see Section 4: Results), it was decided to implement the belt transmitter array. The system architecture for the complete magnetic-based localization proof of concept prototype is shown in Figure 8.
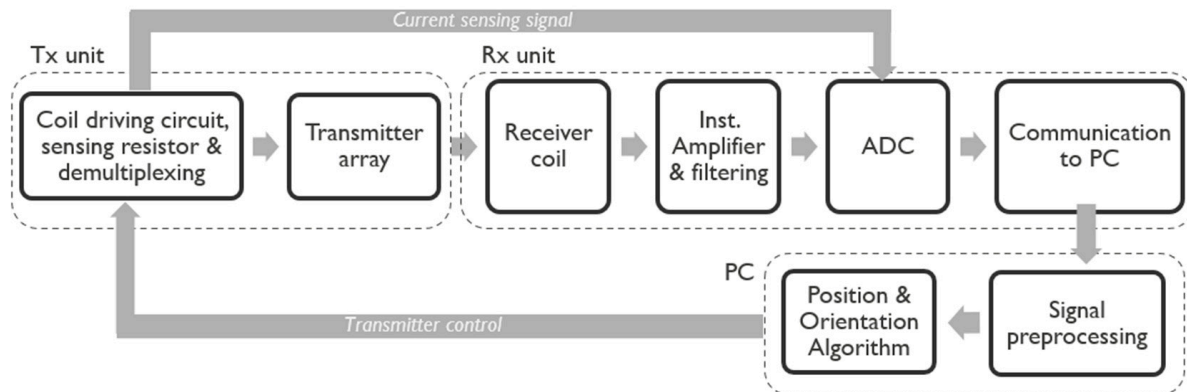

Figure 8. System architecture for the magnetic-based localization proof-of-concept.

3.2.1. Coil Driving and Demultiplexing Stage

The system consists of a coil driving circuit that connects to the transmitter array (either the planar array or the proposed belt array). This circuit includes a half bridge driver that generates a square wave of up to 12 V peak-to-peak (when supplied with 12 V) to be used within an LC series tank circuit consisting of a selected capacitance and each individual coil. A demultiplexing stage is included after the tuning capacitor to time-multiplex the signal for each transmitter coil. Each coil is then grounded via a common 0.1 Ω precision resistor. The voltage at the resistor (after a $\times$ 11 V/V amplification) characterizes the current flowing through each of the coils and detects the sign of the AC magnetic field by means of a phase comparison. Once integrated into a WIC, this sign detection process needs to be updated (since there will be separate controllers for the WIC and the external unit).

A time-multiplexed approach was selected in this case as opposed to frequency multiplexing, as done in [77,81], since the WIC localization requirements allow for a slower localization update, as the movement of the WIC within the GI tract is relatively slow. The fastest speeds within the small intestine have been identified to have upper local values of close to 4.8 mm/s and typical mean progression values of 0.48 mm/s [47]. If the aim is to record location data every 1 cm, then measurements must be performed every 2 s to capture fast movements and every 20 s or higher to capture mean WIC progression. Considering that a complete time-multiplexed acquisition for an eight-coil system takes ~200 ms and a location estimation of ~50 ms (for the optimization settings used in this experiment), the switch to a time-multiplexed system is not expected to introduce additional localization errors when used within a WIC.

This time-multiplexing approach allows the use of the same driver circuit for the complete transmitter array and enables further miniaturization and integration of the system in the future by avoiding the need for individual coil driving circuits. In addition, it reduces the complexity of the WIC circuit and/or digital signal processing regarding the extraction of the signals caused by each transmitter coil. The demultiplexing stage for the planar array was a set of eight relays (PCN-105D3MHZ from TE Connectivity) controlled by a MAX4896ATP+ (Maxim Integrated) relay driver. The relay system for the belt setup was comprised of two stacked PCBs on top of the PCB containing the transmitter circuit (Figure 9), each with four of the same relay drivers connected in daisy chain configuration and controlling 32 relays. An Analog Discovery 2 (AD2) by Digilent® -1300 NE Henley Ct. Suite 3. Pullman, WA, USA- was used to control the stack of boards, allowing for the

definition of the frequency of operation, desired amplitude and the coil activation sequence from a Python script. The same AD2 was used to sequentially acquire both the signal from the 0.1 Ω current-sensing resistor as well as the signal from the receiver coil (see subsection "Receiver coil and signal acquisition"). It is worth noting that in this approach, the signal is not acquired during the switching process, and enough time is allowed for the new signal to stabilize. Hence, the signal transition is not expected to affect the localization results.
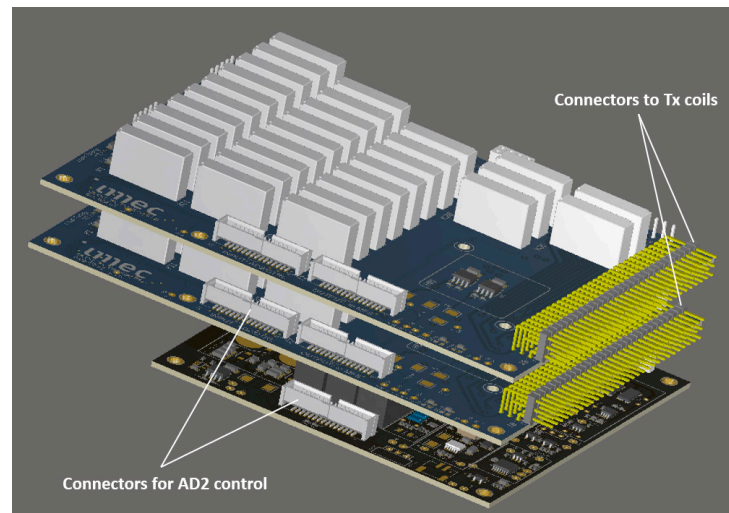

Figure 9. Stacked PCB design including the transmitter (**bottom**) and demultiplexing (**top**) circuits.

The initial choice of using relays instead of CMOS switches was made to ensure full disconnection from all the coils in the transmitter array while aiming to activate an individual coil, as well to allow to use the prototype with a wider range of currents in the transmitter coil in the testing stage. Further integration of the system could make use of more compact CMOS switches, allowing miniaturization of the coil driving unit, provided that the effect of changing the switching characteristics is evaluated for its impact on the localization estimations. Such an impact could be caused by a leakage current flowing into "disconnected" coils, which would add to the magnetic field measured that does not only correspond to the activated coil, resulting in additional noise in the form of a location-dependent magnetic field offset.

3.2.2. Transmitter Arrays

The planar transmitter array (Figure 10a) used for comparison comprised eight PCB coils with an inductance of ~79 μH and a resistance of ~3 Ω, which were spatially distributed in the same way as in [77]. The resistance of a transmitter coil is desired to be as low as possible in order to maximize the transmitter current and obtain a higher LC tank quality factor (4.24 in this case). An equivalent capacitance of 0.5 μF was added in series for a theoretical resonance frequency of 25.32 kHz. The proposed belt array (concept shown in Figure 5b,c) prototype was built with 12 cube three-dimensional coils (3DTX08-A-0060J from Premo Group), each with outer dimensions 14.7 mm $\times$ 16.5 mm $\times$ 11.75 mm around a circular shape with a 36 cm diameter (Figure 10b). The use of such small coils (just above 1 cm in height) has the potential for a minimalistic wearable solution, considering that the number of coils could be reduced, or its distribution could be adapted. The connections to the coil driving and demultiplexing circuit, as well as to the AD2, are shown in Figure 10c.
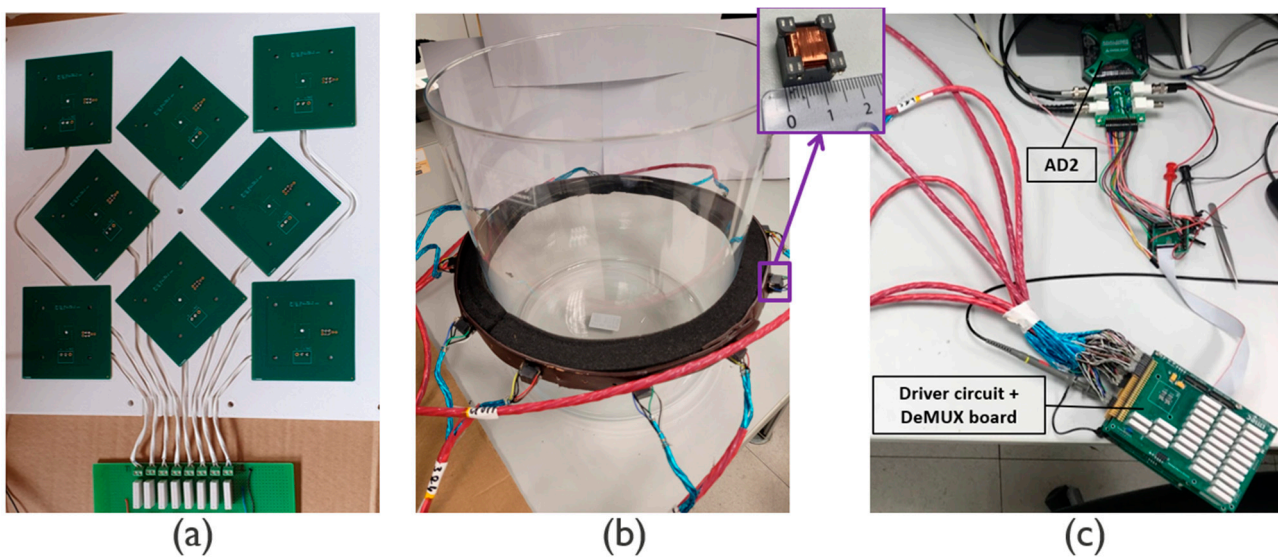
Figure 10. Prototypes used for comparison measurements. (**a**) Planar transmitted array replicated from the available literature; (**b**) belt-transmitter array prototype proposed in this work around a vase simulating the human body; (**c**) transmitting and control circuitry including driver circuit, demultiplexing circuit and an Analog Discovery 2 (Digilent®) controlling unit.

The selection of 12 three-dimensional transmitter units for the proposed belt prototype was based on simulation results, which showed that the obtained localization error did not significantly improve when further increasing this number. These three-dimensional coils have inductances of 100 µH, 100 µH and 78 µH and resistances of 5.4 Ω, 5.6 Ω and 5.6 Ω for the X, Y and Z coils, respectively. Therefore, series resonance capacitors of 400 nF and 520 nF were used for theoretical resonance frequencies of 25.16 kHz and 24.99 kHz. All the system evaluations were done at 25 kHz, and resonance around this frequency was confirmed in measurements. In addition, the current flowing through the coils was characterized for square wave amplitudes between 0.5 V and 10 V. For the presented belt prototype (with 1 A transmitter currents) the transmitter circuit was supplied with 10 V, and current consumptions of 147 mA (transmitter coils off) and 285 mA (transmitter coils on) was observed. This consumption could be further optimized in a later miniaturization stage.

Although this work evaluated these transmitter array prototypes at a frequency of 25 kHz, it is worth mentioning that the choice of frequency may vary as long as it remains within the quasi-static region, does not become significantly attenuated within the body and does not induce significant amounts of Eddy currents that can distort the local magnetic fields. Experiments evaluating these factors have found that an attenuation of 2 dB to 4 dB is already present in the 500 kHz–2 MHz range [84], and that there is an error in the magnetic field of about 5% above 250 kHz [81], with field errors of 2% to 3% already having an impact on a magnetic localization system. Based on this, it is recommended to limit to frequencies below 200 kHz for localization purposes. The choice of frequency should take into account the effects of frequency on receiver sensitivity (lower sensitivity with a decrease in frequency), bandwidth characteristics for readout circuits and the resulting power consumption.

3.2.3. Receiver Coil and Signal Acquisition

In the receiver, a one-dimensional ferrite coil (TP0602-09000J from Premo Group) was used, with dimensions of 6.6 mm × 2.3 mm × 1.75 mm, an inductance of 9 mH, a resistance of 175 Ω and a reported sensitivity of 35 mV/A/m (27.8 mV/µT) at 125 kHz. Considering the linearity of the coil at lower frequencies, the sensitivity at the selected working frequency of 25 kHz is estimated to be 5.56 mV/µT. The coil size allows for its integration within a typical WIC with standard FDA size. This coil was connected to

an instrumentation amplifier and further low-pass filtered (and additionally amplified if required) using an SR560 low noise preamplifier from Stanford Research Systems. The two instrumentation amplifiers included in the evaluation (INA350 from Texas Instruments and MCP6N11-010 from Microchip) were preselected as two options that could potentially be integrated within a WIC due to their size, with trade-offs in power consumption vs. bandwidth (see Table 1). These were supplied with 3 V and a 1.5 V mid-supply reference using a battery-powered supply. The different configurations evaluated in this work, as well as the current through the transmitter coils, are shown in Table 2.

Table 1. Main characteristics of the instrumentation amplifiers used in the receiver part of the presented WIC magnetic-localization proof-of-concept.

Instrumentation Amplifier	Size	Quiescent Current	Bandwidth @ Gain ×50	Available Gain
INA350	2 mm × 2 mm	100 μA	25 kHz	×30, ×50 *
MCP6N11	2 mm × 3 mm	800 μA	100 kHz (GBP: 5 MHz)	≥ ×10

* Limited to ~×35 when working at the 25 kHz bandwidth limit.

Table 2. Transmitter–receiver configurations evaluated in this work, together with the applied current through each of the transmitters.

Transmitter Array	Instrumentation Amplifier/ Theoretical Gain	Current through Coil	Low-Pass Filter/Additional Amplification	Characterized Total Gain	Tested Planes above Transmitter
Planar Transmitter *	INA350/× 50	325 mA	100 kHz, (12 dB/Octave)/× 1	×33	(7–20) cm ***
	MCP6N11/× 50	144 mA	30 kHz, (12 dB/Octave)/× 1	×28	(5–20) cm
Belt Transmitter **	INA350/× 50	1 A	100 kHz, (6 dB/Octave)/× 10	×359	(7.5–20) cm

* Reported configurations performed better than others, possibly because of lowered total gain and/or increased noise; ** Belt experiments limited to INA350 as these aimed for an initial performance comparison; *** Measurements at 5 cm from transmitter were not included since these resulted in amplifier saturation.

In the case of the planar transmitter array, the best performing configurations were reported for each instrumentation amplifier. This resulted in different current and filtering settings between the INA350 and the MCP6N11. This is likely caused by the limited bandwidth of the INA350, which required an increase in the cut-off frequency to limit further gain reduction, resulting in increased noise and requiring a higher signal amplitude to achieve lower errors.

The signal from the individual transmitter coils was sequentially acquired simultaneously with the current sensing signal by the same AD2 (Digilent®) and Python program used to control the coil driving board. It is worth noting that this centralized control of the driving board and signal acquisition was only done for the proof-of-concept prototype, and these two functions need to be performed by separate systems in a realistic WIC setup (namely the WIC and the external controller). Therefore, wireless synchronization between these separate systems, further integration of the receiver circuitry and in-controller amplitude and (relative) sign extraction are necessary as next steps.

3.3. System Evaluation

The system was evaluated using a robot arm (Dobot Magician from Dobot) with a wooden stick attached to its pen holder accessory (Figure 11) to avoid the presence of metallic objects in the surroundings that may distort local magnetic fields. The receiver coil, together with the instrumentation amplifier, was placed at the tip of this stick, and

the signals were connected to the preamplifier and power supply using a USB-C cable and the appropriate connection adapters. The robot arm was placed on an upper shelf, while the transmitter being tested was placed on a table mechanically connected to this shelf, as shown in Figure 11b. A Python script was used to program the robot arm to perform movements within a grid of 7×7 points with X and Y coordinates ranging from -7.5 cm to $+7.5$ cm, resulting in a plane covering 15 cm $\times$ 15 cm. The selection of this plane was limited by the working area of the robot arm. The transmitter array being tested was then placed below the receiver coil with its centre (0,0 coordinates) aligned with the coil.
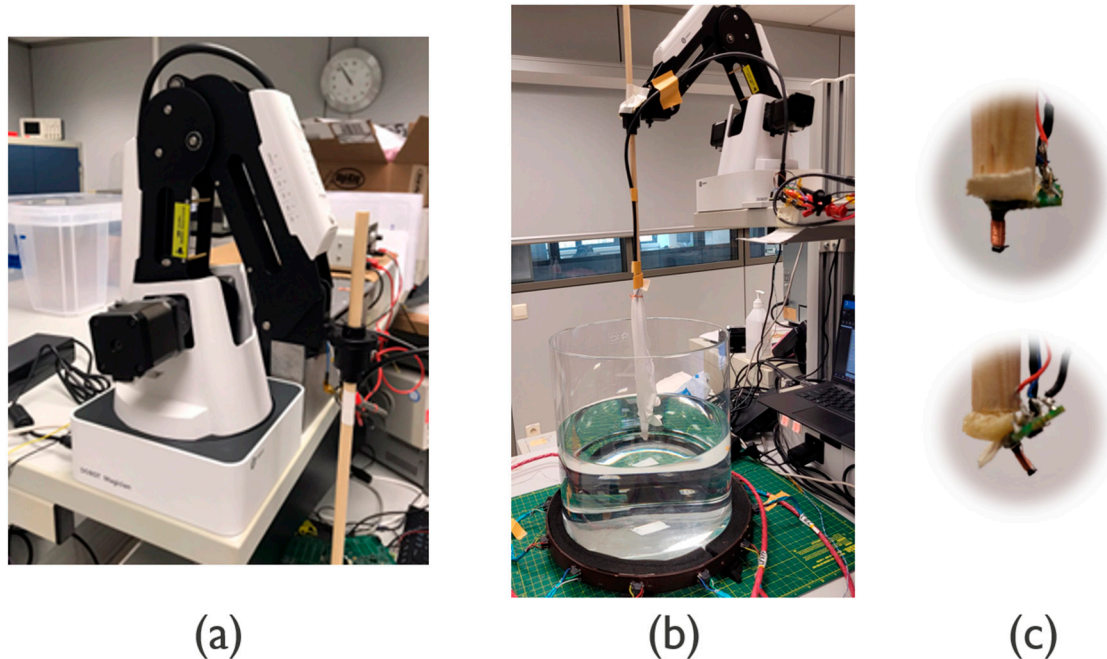

(a) (b) (c)

Figure 11. Reference setup used for the evaluation of the WIC localization prototypes, including a Dobot Magician robot arm used for reference position and receiver coil with instrumentation amplifier PCB. (**a**) Robot arm placed on the top shelf, as used in the experiments. (**b**) Robot arm placed on the top shelf showing complete assembly with a wooden stick. (**c**) Close-up picture of the tip of the wooden stick with the instrumentation amplifier PCB and receiver coil in two different orientations.

A calibration step was included in the protocol, as done in [77]. The data points collected at 12.5 cm from the transmitter were used along with a non-linear least-squares algorithm to determine the amount by which the Biot-Savart model calculations needed to be scaled for a specific coil. These per-coil scaling factors were then stored for a specific setup and further used when performing localization estimations for that and other planes in the volume of interest.

The data collected by a Python script through the AD2 were imported into Matlab® R2018a, where the magnetic field amplitude and phase-based sign were calculated for each coil and each acquisition point. The amplitude extraction was obtained by performing a Fast Fourier Transform (FFT) in ~110 periods of the signal and obtaining the maximum amplitude in the 24.5 kHz–25.5 kHz range, while the sign was based on the phase difference between the current sensing signal obtained from the transmitter circuit and the receiver signal being processed. This data were then fed into the optimization algorithm (implemented by using the 'lsqnonlin' function from Matlab) with an optimization function based on the Biot-Savart law. The implementation of the model followed the calculations presented in [85] for straight current filaments. After obtaining the estimated localization, the Mean Absolute Error (MAE) was calculated for each measured plane.

For the optimization algorithm, boundary conditions were defined for a volume of 25 cm $\times$ 25 cm $\times$ 25 cm. In addition, to consider their possible impact on the accuracy of

the result, three configurable options for initial conditions were included: (1) real location; (2) location 'close' to the real location with a random Gaussian error (means of 8 ± 3 cm and 12 ± 4 cm); (3) 'opposite' location, in which the initial condition is in the same Z plane as the real location but in opposite (multiplied by -1) location in the X and Y dimensions.

In addition to the comparison measurements described above for the planar and belt array transmitters in air, an additional set of measurements were done with the belt array transmitter around a body phantom (Figure 12). The simplified body phantom modelled human tissue conductivity at 25 kHz of 0.2 S/m (based on kidney/liver data from [86]) using an aqueous NaCl solution of 12 mmol/L (based on data for aqueous NaCl solution at 25 °C from [87] and consistent with the characteristics reported at higher frequencies starting at 500 MHz in [88]). The dielectric properties of this simplified body phantom used for the evaluations at quasi-static frequencies did not specifically model those of body tissue, but instead approximated those of water.
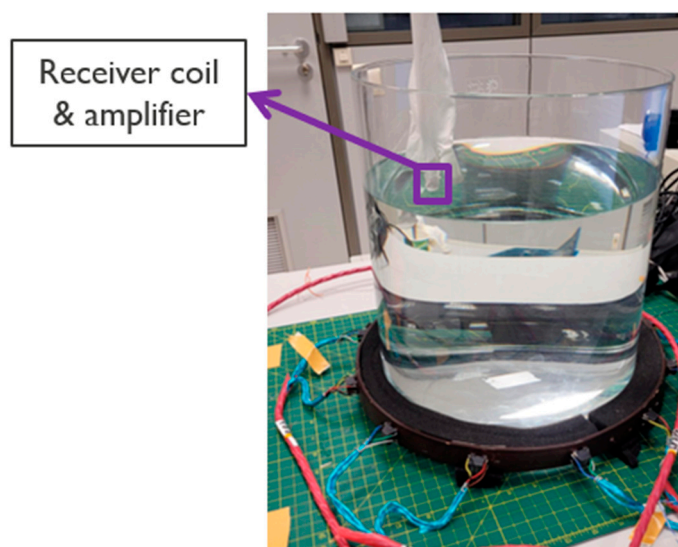

Figure 12. Measurement setup for the belt transmitter array using a simplified body phantom modelling human tissue conductivity at 25 kHz. The receiver coil and amplifier located at the tip of the wooden stick inside a thin protective plastic cover are shown when placed inside the phantom liquid.

4. Results

4.1. Simulation of Wearable Transmitter Concepts

The simulation results for the different wearable transmitter array concepts previously shown in Figure 5 are shown in Figure 13 for magnetic noise levels ranging from 0.001 nT rms to 500 nT rms. To achieve this, white Gaussian noise was added to each simulated magnetic direction, followed by calculating the resulting vector for the simulated Rx orientation ($10°,15°$ in a spherical coordinate system). Measurements were performed to estimate the expected magnetic noise. This was done by acquiring a constant magnetic amplitude (leaving 1 Tx coil active and the Rx coil in the same location), computing the (FFT-based) peak-to-peak magnetic field amplitude and evaluating the AC component of the obtained amplitude for a total of 588 datapoints. This process was repeated 10 times to obtain a representative sample variation across iterations and for two different supports of the receiver coil, namely the robot arm with the wooden stick and on a box on top of the transmitter. The resulting typical magnetic field noise values were in the range of 0.2 nT rms to 1.5 nT rms when evaluated in both the robot setup and the box setup (considered to be a more mechanically stable setting). It was observed that, in some of the measurements, when using the robot setup, the noise level could reach 10.6 nT rms, which highlights some limitations of the reference location system (e.g., prone to vibrations).
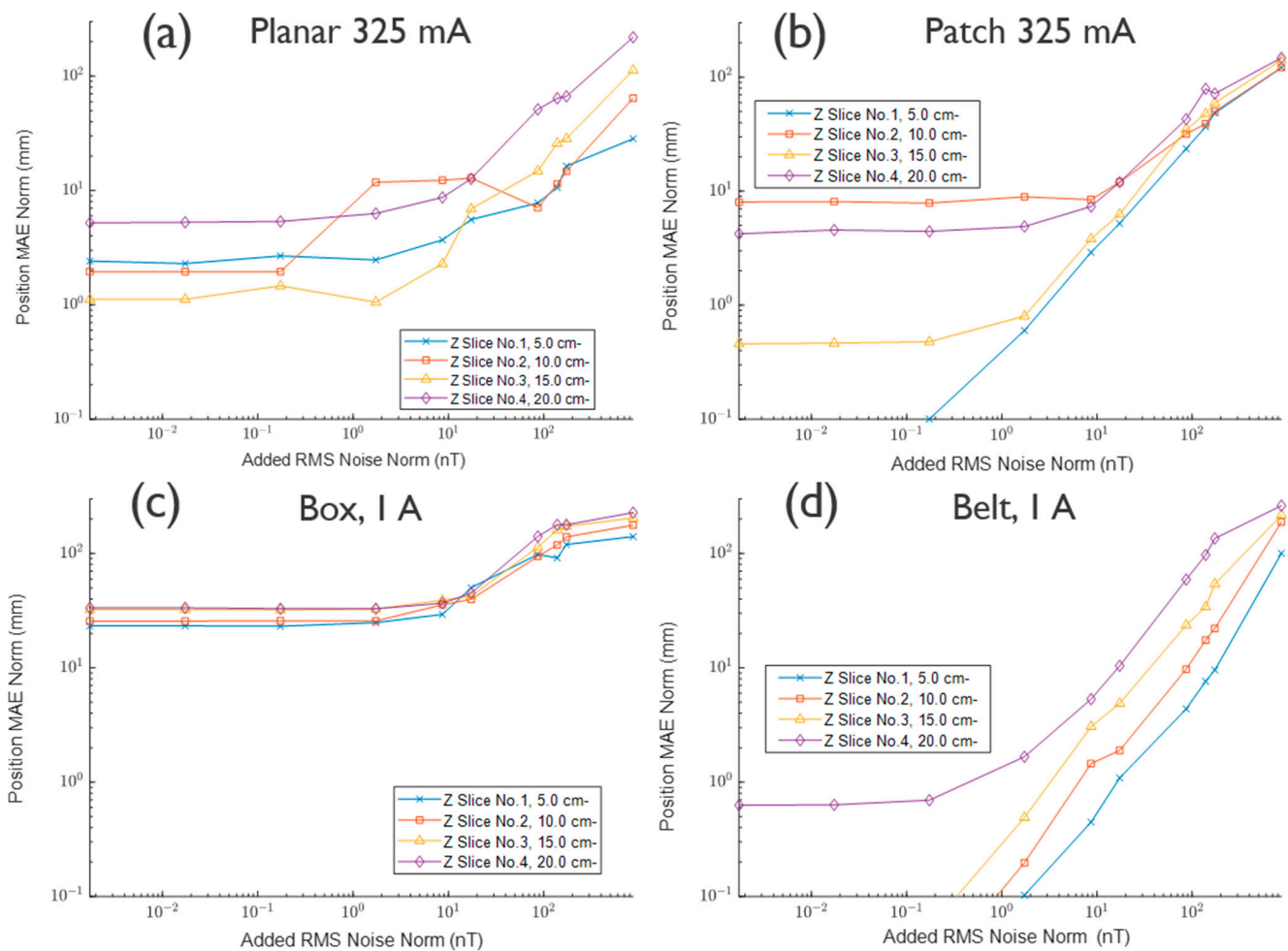
Figure 13. Simulation results for the different wearable transmitter array concepts. (**a**) For a planar transmitter with 325 mA through the 8 one-dimensional coils; (**b**) for a patch transmitter with 325 mA through the 8 one-dimensional coils; (**c**) for a box wearable transmitter with 1 A through the 9 three-dimensional coils; (**d**) for a belt array transmitter with 1 A through the 12 three-dimensional coils. The simulation results shown correspond to "opposite" initial conditions (see Section 3: Methods).

As shown in Figure 13, both the planar and patch systems have the potential to estimate localization with errors below 1 cm for the volume of interest. However, due to the reduced size of the coils and the limited magnetic field amplitude when placed on the subject's waist, the box transmitter concept simulations show errors between 20 mm and 40 mm. The use of a belt with the same three-dimensional coils as in the box significantly improves the localization accuracy due to the spatial distribution of the coils around the volume of interest. In this case, errors below 1 cm can be achieved for the expected noise levels. Therefore, the belt array was selected to be implemented in the wearable proof of concept prototype.

4.2. Simulation Results for the Addition of a Second Receiver Coil

The simulations evaluating the effect of a second receiver coil were limited to the planar transmitter in order to obtain a general idea of the overall added value of such an addition for future implementations. Simulations were carried out using different signal-to-noise ratio (SNR) levels to compare the performance of having only one receiver coil vs. the different approaches when having two coils. These SNR levels were defined with respect to the averaged signal at 1 cm from the transmitter. Simulations were done for SNR between 30 dB and 200 dB, considering that for this specific measure, realistic values

(i.e., comparable to the noise measurements presented in the previous section) are expected to be around 150 dB.

Simulated results, shown in Figure 14, demonstrate that, as expected, the method where the optimization solver has doubled the information as input (correctly adapted for the 90-degree angle of the second receiver) results in better performance in noisy environments than the other two approaches when using two Rx coils. Furthermore, the added value of including a second receiver coil in a noisy environment (versus the case where only one receiver is used) was also seen in these simulations. The decision to include a second coil within a WIC will depend on the available space and the possible magnetic effects between the two receiver coils (i.e., when these have ferrite cores). In addition, it needs to be evaluated whether the limited sensitivity of a second coil (due to the smaller available space in the second dimension) is enough to provide measurements that can improve the overall accuracy.
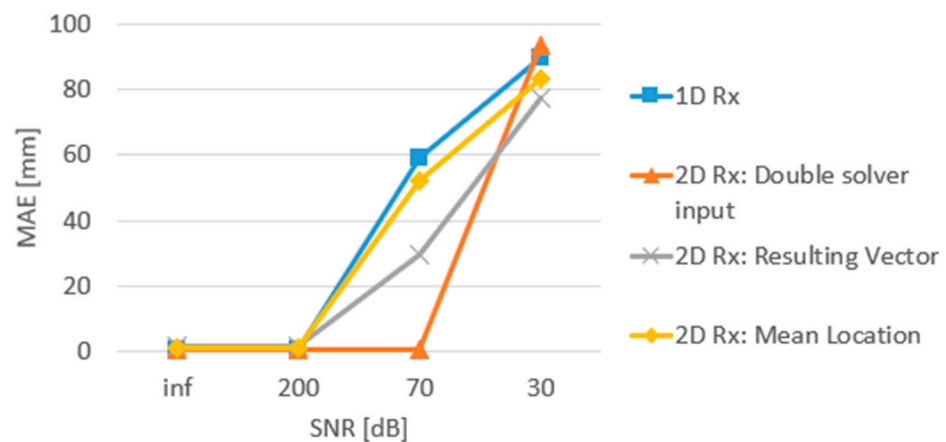

Figure 14. Simulation results for the addition of a second receiver coil within the WIC.

4.3. Measurement Results in Air Medium

The results, which include MAE for the in-air measurements with the combinations of transmitter array and instrumentation amplifier presented in Table 2, are shown in Figures 15 and 16. Each MAE datapoint was obtained from the errors for a 7×7 plane at different heights from the transmitter arrays. The results from the planar setup shown in Figure 15 confirm the potential of such magnetic-based system to achieve sub-cm accuracies, as already reported in literature. This array implementation allowed for achieving a MAE of as low as 6.5 mm in the 15 cm $\times$ 15 cm $\times$ 15 cm volume when using the initial conditions defined as "opposite" (see Section 3: Methods) and the MCP6N11 instrumentation amplifier. These results highlight the possibility of the resulting errors remaining at this level even when reducing the receiver amplification and dynamic range, as was done in this work, which is a necessary adaptation when moving into a WIC form factor. Dynamic ranges of ±15 V, typically presented in these systems [81], are not feasible within a WIC. As mentioned in methodology section and Table 2 the results shown for the two instrumentation amplifiers were obtained using different current and filtering configurations, as these corresponded to lower obtained errors. Volume-averaged MAE values for the INA350 under the same settings as the presented MCP6N11 experiments were in the order of 15 mm (as opposed to 11.5 mm, as in the presented results).
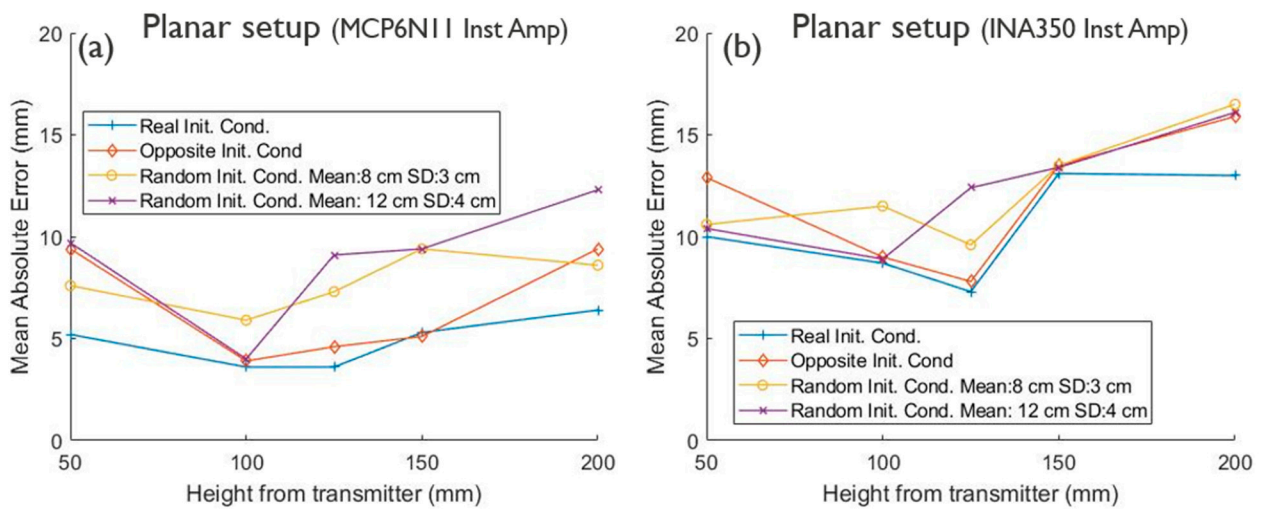
Figure 15. Localization MAE values for the planar transmitter setup. (**a**) MAE values for the receiver configuration with the MCP6N11 instrumentation amplifier and 144 mA through the transmitter coils; (**b**) MAE values for the receiver configuration with the INA350 instrumentation amplifier and 325 mA through the transmitter coils. Measurements correspond to a vertical orientation of the receiver. Reported configurations for each instrumentation amplifier performed better than others, possibly due to lowered total gain and/or increased noise. INA350 evaluations under the same MCP6N11 configurations showed an overall MAE value of 15.4 mm.
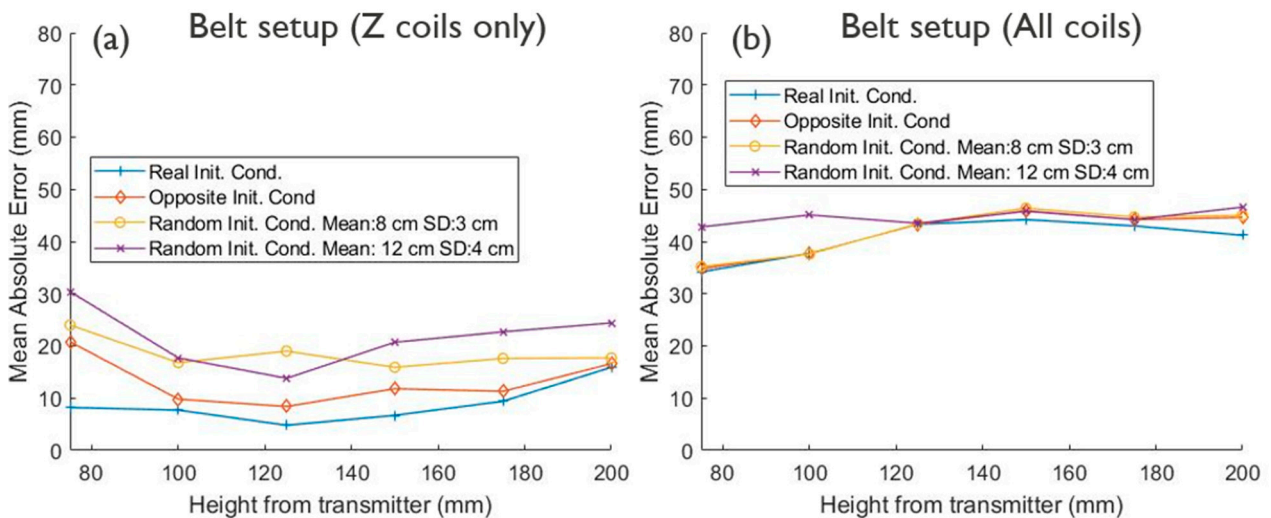

Figure 16. Localization of MAE values for the belt transmitter array setup with receiver configuration using the INA350 instrumentation amplifier and 1 A through the transmitter coils with a vertically oriented receiver coil. (**a**) MAE values when using only the Z coils (aligned with the belt circumference ratio) as input to the localization algorithm; (**b**) MAE values when using all 36 coils from the 12 three-dimensional units as input to the localization algorithm.

These results correspond to a configuration where the receiver coil was in a vertical position with respect to the transmitting plane. This is a restriction that clearly cannot be imposed for a WIC in realistic conditions, and acceptable errors in different orientations should be guaranteed for a useful localization system. When evaluating this system in other orientations, increasing errors were observed with an angle increase with respect to the transmitter plane (e.g., errors between 4 cm and 5 cm with the receiver inclined by 45°). These results contrast with those presented in [81], where the errors remained in the mm range, even with an inclined one-dimensional receiver. It is hypothesized that this may

have been due to the larger amplification factor ($\times 500$ V/V) and dynamic range (30 V) used in that work.

The results from the equivalent (in-air) evaluation of the belt transmitter prototype, which aims to solve the wearability and directionality restrictions by using the small ~1 cm^3 three-dimensional coils, are presented in Figure 16. These results are divided in two scenarios: Figure 16a shows the results when only using the Z component of each three-dimensional transmitter coil (i.e., the coil aligned with the radius of the transmitter circumference), while Figure 16b shows the result when using the complete 36 transmitter coils resulting from 12 three-dimensional coil units. These results (especially Figure 16a) show that the proposed solution has the potential to achieve low enough errors to be used within a WIC application. Specifically, for the evaluated volume of 15 cm $\times$ 15 cm $\times$ 12.5 cm, a MAE of 13.1 mm was achieved when using the initial conditions defined as "opposite" (see Section 3: Methods). Nevertheless, these values were slightly higher than the ones obtained for the planar setup, and most importantly, introducing all the coils in the system (Figure 16b) caused the overall error to increase by approximately 2 cm, resulting in MAE values close to 4 cm. This goes against what would be expected, since an increase in the number (and directionality variation) of transmitter coils would normally have a positive impact on the accuracy of the localization system. These relatively higher error levels are believed to be caused by a discrepancy between the used Biot-Savart model and the real magnetic field values, as will be further explained below.

As with the planar setup, the results shown in Figure 16 were obtained using a vertical orientation of the receiver coil. When measuring with an inclined coil (45° orientation with respect to transmitter plane), the resulting MAE values were as shown in Figure 17. These values show an increase in the error when using only the Z coils (i.e., the coil aligned with the radius of the transmitter circumference), while errors when using all coils remain in the 30–40 mm range.
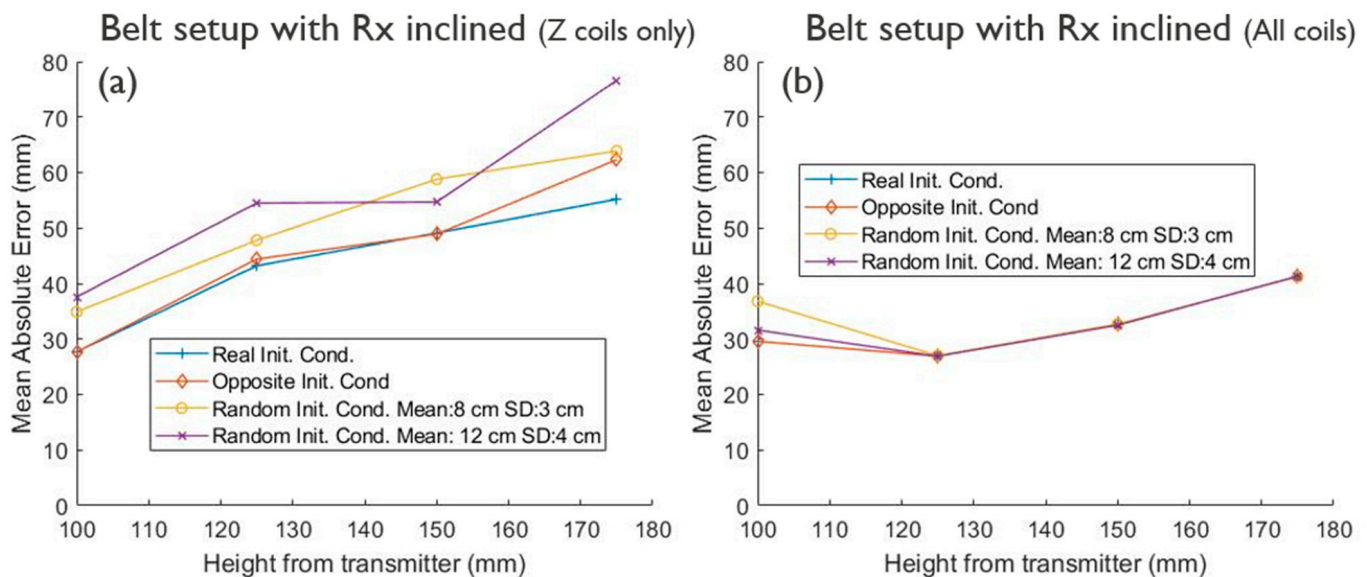

Figure 17. Localization MAE values for the belt transmitter array setup with receiver configuration using the INA350 instrumentation amplifier and 1 A through the transmitter coils, with a receiver coil inclined at 45° with respect to the belt array circumference. (**a**) MAE values when using only the Z coils (aligned with the belt circumference ratio) as inputs to the localization algorithm; (**b**) MAE values when using all the 36 coils from the 12 three-dimensional units as inputs to the localization algorithm.

This increase in error, as well as the relatively high error from Figure 16b, is presumably caused by a mismatch between the magnetic field model used in the optimization algorithm and the actual magnetic field. This is believed to be caused by the Biot-Savart model used [85], not taking into account the magnetic field increase caused by the ferrite core

inside the three-dimensional coil, and only modeling the addition of the individual fields due to each wire segment. To confirm this hypothesis, the theoretical field based on the Biot-Savart law was plotted and compared to the measured data (see example in Figure 18). This comparison includes the theoretical field before and after scaling using the per-coil calibration factors obtained in the calibration step.
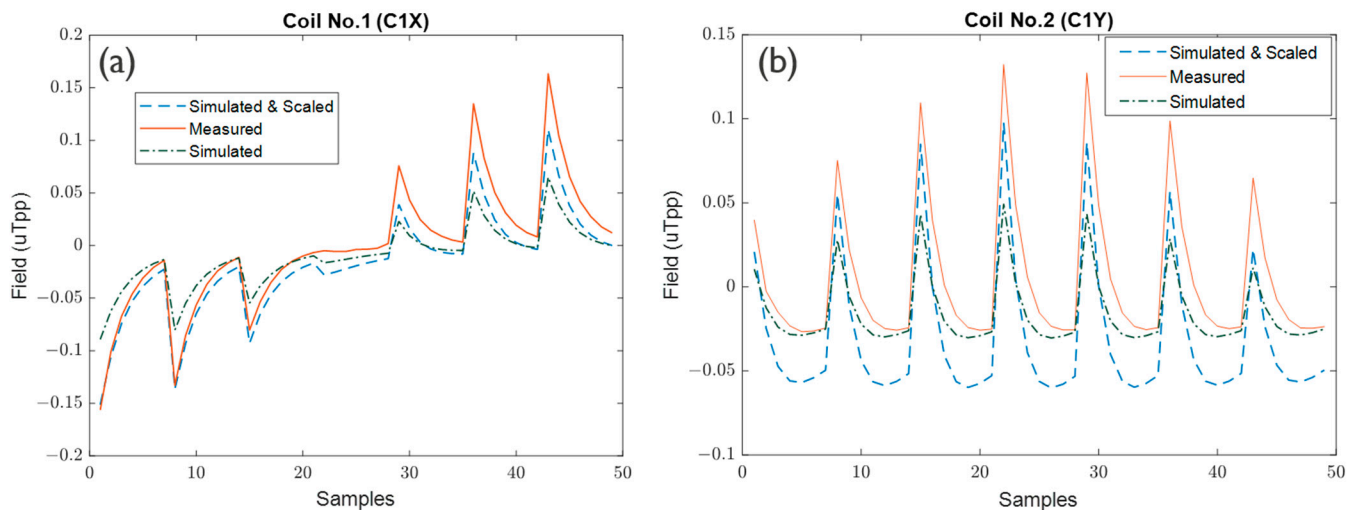

Figure 18. Comparison between the simulated and measured magnetic fields for 49 locations on a specific test plane. (**a**) Example where scaling all the points by a common calibration factor resulted in similar patterns between the measurement and theoretical fields; (**b**) Example where scaling all the points by a common calibration factor resulted in a significant discrepancy in the magnitude field amplitude between the measurement and modelled field.

It is clear from this comparison that, while the magnetic fields at a subset of datapoints (e.g., on one test plane) for some coils (Figure 18a) can be sufficiently precisely approximated using a common scaling factor applied to the original Biot-Savart model, in other cases (Figure 18b), it is not possible to approximate a common scaling factor for all the collected points without introducing large errors. This implies that such a scaling-factor based calibration performed at a middle plane cannot accurately compensate for the magnetic field model over the complete volume of interest and for any possible orientation. A more complex compensation method that takes into account a more precise field distribution of the ferrite-core coils is required to further improve accuracy.

To further confirm this spatial dependency, a simulation using a finite element method (FEM) tool (Using the software Finite Element Method Magnetics [89]) was performed. The ratio (i.e., scaling factor) between the field generated by a coil with and without a ferromagnetic core was computed. For this purpose, a two-dimensional simulation of a solenoid with an iron core (rectangle in Figure 19a) was done, and the field magnitude along the vertical axis at the center of the solenoid was computed (Figure 19b) along with the scaling factor. The results indicate that this scaling factor can be between 2 and 3 for fields outside the core (corresponding to the distances 0–5 cm and 10–15 cm in the simulation). For the actual three-dimensional coils used in the belt array, the scaling factors were estimated using the least-squares optimization algorithm over a comparable range from 1.2 to 4.
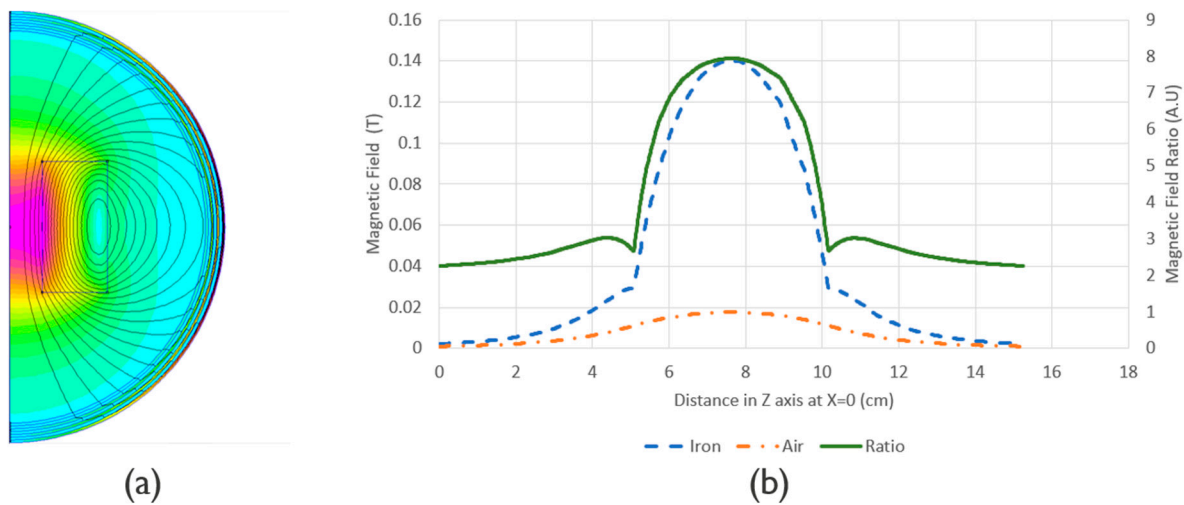
(a)

(b)

Figure 19. Finite element simulation comparing the magnetic field from a coil with a ferromagnetic core against one with an air core. (**a**) Simulation space with the rectangle corresponding to a cross section of a solenoid with an iron core; (**b**) magnetic field results and ratio between the two scenarios, showing that there is a position-dependent ratio varying between 2 and 3 for this specific example case.

4.4. Measurement Results in Simplified Body Phantom

The results for the additional set of measurements from the belt transmitter array around a simplified body phantom are shown in Figure 20. These measurements were performed for a vertically oriented receiver coil and show comparable results to the equivalent in-air measurements in Figure 16. This serves as an additional confirmation of the advantages of using quasi-static electromagnetic signals due to the 'transparency' of the human body (i.e., similar permeability to that of air) to these fields.
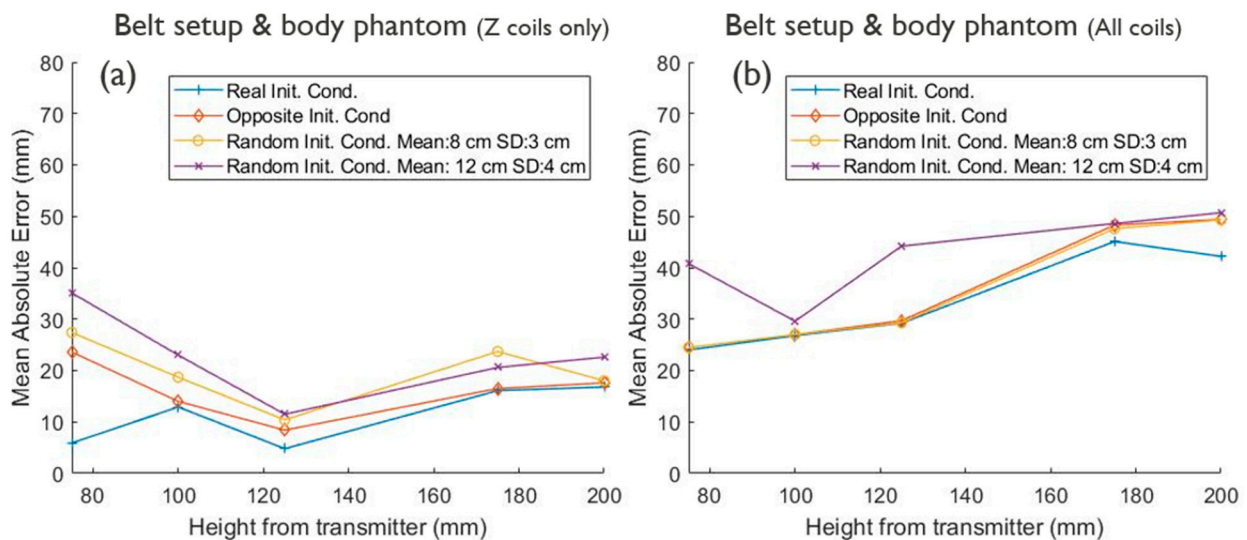

Figure 20. Localization MAE values for the belt transmitter array setup when evaluated around a body phantom (receiver configuration using the INA350 instrumentation amplifier and 1 A through the transmitter coils, with a vertically oriented receiver coil). (**a**) MAE values when using only the Z coils (aligned with the belt circumference ratio) as input to the localization algorithm; (**b**) MAE values when using all the 36 coils from the 12 three-dimensional units as inputs to the localization algorithm.

5. Discussion

This work presents a proof-of-concept WIC localization system that aims to overcome the wearability limitations of systems typically found in the literature. To achieve this goal, simulations of different magnetic transmitter concepts with increased wearability were performed. Based on these simulations, it was decided to build a prototype which included a belt array containing three-dimensional coils with ferrite cores. In addition, an evaluation of the effect of including a second receiver coil in the WIC was conducted. The simulation results showed that there is a clear advantage in including such a second receiver inside the WIC. However, this needs to be further evaluated experimentally, and the choice should consider factors such as the interaction between receiver coils (when including ferrite cores), available space and need for multi-channel or multiplexed receiver circuits within the WIC, among others.

Although the results from the planar transmitter showed slightly higher localization errors than those reported for similar systems, it was shown that even with a reduced gain and dynamic range, it is possible to obtain localization estimations with errors close to 1 cm. Receiver circuits with two instrumentation amplifiers, which are potentially usable within a WIC, were evaluated. These circuits presented a tradeoff between available bandwidth and power consumption. Therefore, the evaluation of the INA350 amplifier required the use of higher transmitter current and a higher low-pass cutoff frequency to reduce the impact of gain reduction caused by its limited bandwidth, which in turn increases the noise of the signal.

Although the results from the planar transmitter shown in Figure 15 show that the MCP6N11 can potentially allow for slightly lower errors and higher gains than the INA350, this implies a tradeoff in power consumption. The selection of the amplification stage should be done considering the available power for the WIC, the space used and the transmitter characteristics required to achieve an acceptable error for different WIC orientations. Given the necessary model improvements identified in this work, the selection and an additional evaluation of the complete system should be done after updating the algorithm with a more accurate model that represents the field generated by the transmitter coils with a ferrite core.

The increase in error when evaluating the planar setup in orientations other than vertical (possibly caused by the reduction of gain and dynamic ratio) highlights the need to use a transmitter that contains compact coils with different orientations (e.g., the proposed three-dimensional cubes) not only for improved wearability, but also as a compensation mechanism for the limitations in amplification and dynamic range when including a receiver system within a WIC. These results, together with the wearability limitations found in literature, led to the selection of three-dimensional coil cubes for the proposed belt array.

It was found that a transmitter with a belt-shaped array of three-dimensional coils, such as the one proposed in this work, can help to overcome these limitations, as comparable errors to the planar setup were found. Furthermore, the validation using a simplified body phantom served as an additional indication of the transparency of the human body to quasi-static magnetic fields and the well-documented advantage of magnetic-based localization methods compared to RF-based techniques.

Despite this, it was clear from the obtained belt array results that the localization estimation using such a wearable prototype would greatly benefit from a more accurate model that includes the effects of having a ferromagnetic core in the transmitter coils. This is evident in the evaluation of the data presented in Figure 18 and the FEM simulation shown in Figure 19, from which it can be concluded that the use of the Biot-Savart law together with a calibrated coil-specific scaling factor is not enough to accurately model the effects of the ferrite core. Based on this, it is expected that a more accurate model of these coils will result in a lower localization error. Therefore, the next steps could involve the use of techniques such as the addition of current filaments to the model that would represent the generated currents in the ferrite, or the use of a point dipole source model. In the case

of the addition of model current filaments, iterative approaches based on FEM simulations and/or characterization measurements could be used to find the optimal distribution of filament locations and current amplitudes within the model. This, in combination with additional experiments, can be used to validate that the obtained localization estimations have acceptable errors that are maintained for different WIC orientations.

Furthermore, additional modifications to the system are required to translate this concept into a specific WIC implementation. This includes a method to extract the magnitude and (relative) sign of the acquired signals that does not depend on a common controller for the transmitter (wearable belt) and receiver (the WIC) units. In addition, it is possible that the limited dynamic range within the WIC, together with the third-order exponential decrease in the magnetic signal, would require real-time adaptations in gain, receiver tuning or other parameters in order to guarantee the performance of the WIC localization system in the volume of interest and for random orientations. The specific characteristics of these implementations will depend on the performance of the selected transmitter, along with an updated magnetic model.

When considering a realistic environment, it is also important to consider non-circular belt shapes that follow the varying anatomical body shapes. The effects of relative motion (depending on whether the belt is worn at the waist or at the chest level) may also need to be corrected using compensation algorithms, possibly in combination with additional receiver device(s) placed on the subject's torso and abdomen.

In addition to the model mismatch, additional error may have been introduced in the reported results by errors from the reference location. For example, vibrations in the robot arm can introduce additional noise, and robot positioning errors of approximately 2 mm were identified even after performing the manufacturer-recommended calibration. Nevertheless, the main source of error in the results shown for the belt transmitter array remains the difference between the modelled air coils and the magnetic field generated by the coils with ferrite cores. To improve accuracy in this regard, a possible solution could be the use of a robot arm with greater precision, together with a setup with a more controlled configuration (minimizing the possible vibrations). Alternatively, a mechanical setup with manual movement between points could be used, although this would increase the time required for performing measurements in the complete volume of interest.

6. Conclusions

The presented work aimed to overcome the wearability limitations of magnetic-based WIC localization systems. After simulation of different concepts with increased wearability, a proof-of-concept belt array transmitter was built and evaluated. The results showed the potential of such a wearable array to perform WIC localization with MAE errors within the range of 10–25 mm, which were comparable with the sub-cm errors obtained by reproducing a planar transmitter array with reduced gain and dynamic range in the receiver side. Despite these promising results, it was found that improvements to the model when using transmitter coils with a ferrite core are necessary. These are expected to further decrease the WIC localization errors and enable the use of magnetic-based localization systems in ambulatory settings; a functionality that is gaining importance given the recent advances in WICs with multiple sensing capabilities.

Author Contributions: Conceptualization, I.C., T.T. and J.W.d.W.; methodology, I.C., J.W.d.W., J.v.V., T.V.Q. and W.H.; software, I.C., J.v.V., T.V.Q. and W.H.; validation, I.C., J.v.V., T.V.Q. and W.H.; formal analysis, I.C., T.T., J.W.d.W., J.v.V., T.V.Q. and W.H.; investigation, I.C., T.T., J.W.d.W., J.v.V., T.V.Q. and W.H.; resources, T.T.; data curation, I.C.; writing—original draft preparation, I.C.; writing—review and editing, I.C., T.T., J.W.d.W., J.v.V., T.V.Q. and W.H.; visualization, I.C.; supervision, T.T., J.W.d.W. and I.C.; project administration, T.T. All authors have read and agreed to the published version of the manuscript.

References

1. Medtronic. PillCam SB 3 Capsule Endoscopy System. Available online: https://www.medtronic.com/covidien/en-us/products/capsule-endoscopy/pillcam-sb3-system.html (accessed on 28 March 2023).
2. Olympus. Endocapsule 10 System. Available online: https://www.olympus-europa.com/medical/en/Products-and%20Solutions/Products/Product/ENDOCAPSULE-10-System.html#:~:text=The%20ENDOCAPSULE%2010%20System%20is,accurate%20observations%20and%20reliable%20diagnoses (accessed on 28 March 2023).
3. CapsoVision. CapsoCam System. Available online: https://capsovision.com/capsocam-system/ (accessed on 28 March 2023).
4. IntroMedic. MiroCam Capsule Endoscope System. Available online: http://www.intromedic.com/eng/item/item_010100_view.asp?search_kind=&gotopage=1&no=3 (accessed on 28 March 2023).
5. Jinshan Group. OMOM HD Capsule Endoscopy Platform. Available online: https://www.jinshangroup.com/solutions/omom-hd-capsule-endoscopy-camera/ (accessed on 28 March 2023).
6. Medtronic. SmartPill Motility Testing System. Available online: https://www.medtronic.com/covidien/en-gb/products/motility-testing/smartpill-motility-testing-system.html# (accessed on 2 April 2023).
7. Atmo Biosciences. Introducing the Atmo Gas-Sensing Capsule. Available online: https://atmobiosciences.com/ (accessed on 28 March 2023).
8. Caffrey, C.M.; Twomey, K.; Ogurtsov, V.I. Development of a wireless swallowable capsule with potentiostatic electrochemical sensor for gastrointestinal track investigation. *Sens. Actuators B Chem.* **2015**, *218*, 8–15. [CrossRef]
9. Kimura, T.; Muguruma, N.; Ito, S.; Okamura, S.; Imoto, Y.; Miyamoto, H.; Kaji, M.; Kudo, E. Infrared fluorescence endoscopy for the diagnosis of superficial gastric tumors. *Gastrointest. Endosc.* **2007**, *66*, 37–43. [CrossRef]
10. Biora Therapeutics. Targeted & Systemic Therapeutics. Available online: https://www.bioratherapeutics.com/?utm_source=pr&utm_medium=referral&utm_campaign=precision_med&utm_term=progenity-inc&utm_content=102919 (accessed on 28 March 2023).
11. Mimee, M.; Nadeau, P.; Hayward, A.; Carim, S.; Flanagan, S.; Jerger, L.; Collins, J.; McDonnell, S.; Swartwout, R.; Citorik, R.J.; et al. An ingestible bacterial-electronic system to monitor gastrointestinal health. *Science* **2018**, *360*, 915–918. [CrossRef] [PubMed]
12. Rezaei Nejad, H.; Oliveira, B.C.M.; Sadeqi, A.; Dehkharghani, A.; Kondova, I.; Langermans, J.A.M.; Guasto, J.S.; Tzipori, S.; Widmer, G.; Sonkusale, S.R. Ingestible Osmotic Pill for In Vivo Sampling of Gut Microbiomes. *Adv. Intell. Syst.* **2019**, *1*, 1900053. [CrossRef]
13. Van Helleputte, N.; Even, A.J.G.; Leonardi, F.; Stanzione, S.; Song, M.; Garripoli, C.; Sijbers, W.; Liu, Y.-H.; Van Hoof, C. Miniaturized Electronic Circuit Design Challenges for Ingestible Devices. *J. Microelectromech. Syst.* **2020**, *29*, 645–652. [CrossRef]
14. McCaffrey, C.; Chevalerias, O.; O'Mathuna, C.; Twomey, K. Swallowable-Capsule Technology. *IEEE Pervasive Comput.* **2008**, *7*, 23–29. [CrossRef]
15. Basar, M.R.; Malek, F.; Juni, K.M.; Idris, M.S.; Saleh, M.I.M. Ingestible wireless capsule technology: A review of development and future indication. *Int. J. Antennas Propag.* **2012**, *2012*, 807165. [CrossRef]
16. Zeising, S.; Thalmayer, A.S.; Lubke, M.; Fischer, G.; Kirchner, J. Localization of Passively Guided Capsule Endoscopes—A Review. *IEEE Sens. J.* **2022**, *22*, 20138–20155. [CrossRef]
17. Ye, Y.; Pahlavan, K.; Bao, G.; Swar, P.; Ghaboosi, K. Comparative performance evaluation of RF localization for wireless capsule endoscopy applications. *Int. J. Wirel. Inf. Netw.* **2014**, *21*, 208–222. [CrossRef]
18. Wang, Y.; Fu, R.; Ye, Y.; Khan, U.; Pahlavan, K. Performance bounds for RF positioning of endoscopy camera capsules. In Proceedings of the 2011 IEEE Topical Conference on Biomedical Wireless Technologies, Networks, and Sensing Systems, Phoenix, AZ, USA, 16–19 January 2011; pp. 71–74. [CrossRef]
19. Li, S.; Geng, Y.; He, J.; Pahlavan, K. Analysis of three-dimensional maximum likelihood algorithm for capsule endoscopy localization. In Proceedings of the 2012 5th International Conference on Biomedical Engineering and Informatics, Chongqing, China, 16–18 October 2012; pp. 721–725.
20. Bianchi, F.; Masaracchia, A.; Shojaei Barjuei, E.; Menciassi, A.; Arezzo, A.; Koulaouzidis, A.; Stoyanov, D.; Dario, P.; Ciuti, G. Localization strategies for robotic endoscopic capsules: A review. *Expert Rev. Med. Devices* **2019**, *16*, 381–403. [CrossRef]
21. Wang, L.; Hu, C.; Tian, L.; Li, M.; Meng, M.Q.-H. A novel radio propagation radiation model for location of the capsule in GI tract. In Proceedings of the 2009 IEEE International Conference on Robotics and Biomimetics (ROBIO), Guilin, China, 19–23 December 2009; pp. 2332–2337.

22. Makarov, S.N.; Khan, U.I.; Islam, M.M.; Ludwig, R.; Pahlavan, K. On accuracy of simple FDTD models for the simulation of human body path loss. In Proceedings of the 2011 IEEE Sensors Applications Symposium, San Antonio, TX, USA, 22–24 February 2011; pp. 18–23.
23. Van De Steene, T.; Tanghe, E.; Vermeeren, G.; Torfs, T.; Castro, I.; de Wit, J.W.; Martens, L.; Joseph, W. Robust Radiofrequency Localization in highly heterogeneous environments during Wireless Capsule Endoscopy. In Proceedings of the 44th Annual International Conference of the IEEE Engineering in Meedicine and Biology Society (EMBS), Glasgow, UK, 11–15 July 2022.
24. Anzai, D.; Kato, T.; Wang, J. Theoretical and experimental analyses on location/channel parameters estimation for implantable medical devices. *Electron. Lett.* **2017**, *53*, 1350–1352. [CrossRef]
25. Barbi, M.; Garcia-Pardo, C.; Nevarez, A.; Pons Beltran, V.; Cardona, N. UWB RSS-Based Localization for Capsule Endoscopy Using a Multilayer Phantom and In Vivo Measurements. *IEEE Trans. Antennas Propag.* **2019**, *67*, 5035–5043. [CrossRef]
26. Fischer, D.; Schreiber, R.; Levi, D.; Eliakim, R. Capsule endoscopy: The localization system. *Gastrointest. Endosc. Clin. N. Am.* **2004**, *14*, 25–31. [CrossRef]
27. Marya, N.; Karellas, A.; Foley, A.; Roychowdhury, A.; Cave, D. Computerized 3-dimensional localization of a video capsule in the abdominal cavity: Validation by digital radiography. *Gastrointest. Endosc.* **2014**, *79*, 669–674. [CrossRef]
28. Pourhomayoun, M.; Jin, Z.; Fowler, M.L. Accurate localization of in-body medical implants based on spatial sparsity. *IEEE Trans. Biomed. Eng.* **2014**, *61*, 590–597. [CrossRef]
29. Khan, U.; Ye, Y.; Aisha, A.-U.; Swar, P.; Pahlavan, K. Precision of EM Simulation Based Wireless Location Estimation in Multi-Sensor Capsule Endoscopy. *IEEE J. Transl. Eng. Health Med.* **2018**, *6*, 1800411. [CrossRef]
30. Nafchi, A.R.; Goh, S.T.; Zekavat, S.A.R. Circular arrays and inertial measurement unit for DOA/TOA/TDOA-based endoscopy capsule localization: Performance and complexity investigation. *IEEE Sens. J.* **2014**, *14*, 3791–3799. [CrossRef]
31. Goh, S.T.; Reza Zekavat, S.A.; Pahlavan, K. DOA-Based Endoscopy Capsule Localization and Orientation Estimation via Unscented Kalman Filter. *IEEE Sens. J.* **2014**, *14*, 3819–3829. [CrossRef]
32. Ito, T.; Anzai, D.; Wang, J. Novel joint TOA/RSSI-based WCE location tracking method without prior knowledge of biological human body tissues. In Proceedings of the 2014 36th Annual International Conference of the IEEE Engineering in Medicine and Biology Society, Chicago, IL, USA, 26–30 August 2014; pp. 6993–6996.
33. Sorriento, A.; Porfido, M.B.; Mazzoleni, S.; Calvosa, G.; Tenucci, M.; Ciuti, G.; Dario, P. Optical and Electromagnetic Tracking Systems for Biomedical Applications: A Critical Review on Potentialities and Limitations. *IEEE Rev. Biomed. Eng.* **2020**, *13*, 212–232. [CrossRef]
34. Wille, A.; Broll, M.; Winter, S. Phase difference based RFID navigation for medical applications. In Proceedings of the 2011 IEEE International Conference on RFID, Orlando, FL, USA, 12–14 April 2011; pp. 98–105.
35. Varian Medical Systems Inc. Improving the Accuracy of Raiotherapy Using the Calypso System. Available online: https://www.varian.com/why-varian/improving-accuracy-radiotherapy-using-calypso-system#:~:text=Varian\T1\textquoterights-Calypso-systemand,efficientpatientsetupduringradiotherapy (accessed on 28 March 2023).
36. Ye, J.; Cao, D.; Wong, T.; Shepard, D. Real-time Target Tracking with Calypso 4D Tracking System. Available online: https://www.aapm.org/meetings/amos2/pdf/34-8075-83849-634.pdf (accessed on 28 March 2023).
37. Hashi, S.; Yabukami, S.; Kanetaka, H.; Ishiyama, K.; Arai, K.I. Wireless magnetic position-sensing system using optimized pickup coils for higher accuracy. *IEEE Trans. Magn.* **2011**, *47*, 3542–3545. [CrossRef]
38. Hashi, S.; Toyoda, M.; Yabukami, S.; Ishiyama, K.; Okazaki, Y.; Arai, K.I.; Kanetaka, H. Wireless magnetic motion capture system using multiple LC resonant magnetic markers with high accuracy. *Sens. Actuators A Phys.* **2008**, *142*, 520–527. [CrossRef]
39. Dey, N.; Ashour, A.S.; Shi, F.; Sherratt, R.S. Wireless Capsule Gastrointestinal Endoscopy: Direction-of-Arrival Estimation Based Localization Survey. *IEEE Rev. Biomed. Eng.* **2017**, *10*, 2–11. [CrossRef] [PubMed]
40. Dimas, G.; Spyrou, E.; Iakovidis, D.K.; Koulaouzidis, A. Intelligent visual localization of wireless capsule endoscopes enhanced by color information. *Comput. Biol. Med.* **2017**, *89*, 429–440. [CrossRef] [PubMed]
41. Figueiredo, I.N.; Leal, C.; Pinto, L.; Figueiredo, P.N.; Tsai, R. Hybrid multiscale affine and elastic image registration approach towards wireless capsule endoscope localization. *Biomed. Signal Process. Control* **2018**, *39*, 486–502. [CrossRef]
42. Iakovidis, D.K.; Dimas, G.; Karargyris, A.; Bianchi, F.; Ciuti, G.; Koulaouzidis, A. Deep Endoscopic Visual Measurements. *IEEE J. Biomed. Health Inform.* **2019**, *23*, 2211–2219. [CrossRef] [PubMed]
43. Aghanouri, M.; Ghaffari, A.; Dadashi, N. Image-based localization of the active wireless capsule endoscope inside the stomach. In Proceedings of the 2017 IEEE EMBS International Conference on Biomedical & Health Informatics (BHI), Orlando, FL, USA, 16–19 February 2017; pp. 13–16.
44. Vagner, I.D.; Lembrikov, B.I.; Wyder, P. Quasi-static Electromagnetic Field. In *Electrodynamics of Magnetoactive Media*; Springer: Berlin/Heidelberg, Germany, 2004; pp. 68–81.
45. Schlageter, V.; Drljaca, P.; Popovic, R.S.; Kučera, P. A magnetic tracking system based on highly sensitive integrated hall sensors. *JSME Int. J. Ser. C Mech. Syst. Mach. Elem. Manuf.* **2002**, *45*, 967–973. [CrossRef]
46. Hedsund, C.; Joensson, I.M.; Gregersen, T.; Fynne, L.; Schlageter, V.; Krogh, K. Magnet tracking allows assessment of regional gastrointestinal transit times in children. *Clin. Exp. Gastroenterol.* **2013**, *6*, 201–208. [CrossRef]
47. WorsØe, J.; Fynne, L.; Gregersen, T.; Schlageter, V.; Christensen, L.A.; Dahlerup, J.F.; Rijkhoff, N.J.M.; Laurberg, S.; Krogh, K. Gastric transit and small intestinal transit time and motility assessed by a magnet tracking system. *BMC Gastroenterol.* **2011**, *11*, 145. [CrossRef] [PubMed]

48. Hiroz, P.; Schlageter, V.; Givel, J.C.; Kucera, P. Colonic movements in healthy subjects as monitored by a magnet tracking system. *Neurogastroenterol. Motil.* **2009**, *21*, 838-e57. [CrossRef]

49. Stathopoulos, E.; Schlageter, V.; Meyrat, B.; De Ribaupierre, Y.; Kucera, P. Magnetic pill tracking: A novel non-invasive tool for investigation of human digestive motility. *Neurogastroenterol. Motil.* **2005**, *17*, 148–154. [CrossRef]

50. Haase, A.M.; Gregersen, T.; Schlageter, V.; Scott, M.S.; Demierre, M.; Kucera, P.; Dahlerup, J.F.; Krogh, K. Pilot study trialling a new ambulatory method for the clinical assessment of regional gastrointestinal transit using multiple electromagnetic capsules. *Neurogastroenterol. Motil.* **2014**, *26*, 1783–1791. [CrossRef]

51. Zeising, S.; Anzai, D.; Thalmayer, A.; Fischer, G.; Kirchner, J. Evaluation of the Impact of Static Interference on an Empirical Data Based Static Magnetic Localization Setup for Capsule Endoscopy. *Curr. Dir. Biomed. Eng.* **2020**, *6*, 66–69. [CrossRef]

52. Merino, J.L.; Kazanc, O.; Brunner, N.; Schlageter, V.; Demierre, M.; Dehollain, C. Pediatric Size Swallowable Glass Pill for Digestive Motility Analysis. In Proceedings of the 2018 IEEE International Symposium on Circuits and Systems (ISCAS), Florence, Italy, 27–30 May 2018. [CrossRef]

53. Merino, J.L.; Kazanc, O.; Brunner, N.; Schlageter, V.; Demierre, M.; Dehollain, C. Low power receiver for magnetic digestive motility tracking pill. In Proceedings of the 2015 IEEE International Symposium on Circuits and Systems (ISCAS), Lisbon, Portugal, 24–27 May 2015; pp. 469–472. [CrossRef]

54. Pham, D.M.; Aziz, S.M. A real-time localization system for an endoscopic capsule using magnetic sensors. *Sensors* **2014**, *14*, 20910–20929. [CrossRef]

55. Hu, C.; Meng, M.Q.; Mandal, M. Efficient magnetic localization and orientation technique for capsule endoscopy. In Proceedings of the 2005 IEEE/RSJ International Conference on Intelligent Robots and Systems, Edmonton, AB, Canada, 2–6 August 2005; pp. 628–633. [CrossRef]

56. Hu, C.; Li, M.; Song, S.; Yang, W.; Zhang, R.; Meng, M.Q.H. A Cubic 3-Axis Magnetic Sensor Array for Wirelessly Tracking Magnet Position and Orientation. *IEEE Sens. J.* **2010**, *10*, 903–913. [CrossRef]

57. Hu, C.; Ren, Y.; You, X.; Yang, W.; Song, S.; Xiang, S.; He, X.; Zhang, Z.; Meng, M.Q.H. Locating Intra-Body Capsule Object by Three-Magnet Sensing System. *IEEE Sens. J.* **2016**, *16*, 5167–5176. [CrossRef]

58. Shao, G.; Tang, Y.; Tang, L.; Dai, Q.; Guo, Y.X. A Novel Passive Magnetic Localization Wearable System for Wireless Capsule Endoscopy. *IEEE Sens. J.* **2019**, *19*, 3462–3472. [CrossRef]

59. Wu, X.; Hou, W.; Peng, C.; Zheng, X.; Fang, X.; He, J. Wearable magnetic locating and tracking system for MEMS medical capsule. *Sens. Actuators A Phys.* **2008**, *141*, 432–439. [CrossRef]

60. Dai, H.; Hu, C.; Su, S.; Lin, M.; Song, S. Geomagnetic Compensation for the Rotating of Magnetometer Array During Magnetic Tracking. *IEEE Trans. Instrum. Meas.* **2019**, *68*, 3379–3386. [CrossRef]

61. Wang, M.; Song, S.; Liu, J.; Meng, M.Q.-H. Multipoint Simultaneous Tracking of Wireless Capsule Endoscope Using Magnetic Sensor Array. *IEEE Trans. Instrum. Meas.* **2021**, *70*, 7502510. [CrossRef]

62. Song, S.; Wang, S.; Yuan, S.; Wang, J.; Liu, W.; Meng, M.Q.H. Magnetic Tracking of Wireless Capsule Endoscope in Mobile Setup Based on Differential Signals. *IEEE Trans. Instrum. Meas.* **2021**, *70*, 4005208. [CrossRef]

63. Zeising, S.; Chen, L.; Thalmayer, A.; Lübke, M.; Fischer, G.; Kirchner, J. Tracking the Traveled Distance of Capsule Endoscopes along a Gastrointestinal-Tract Model Using Differential Static Magnetic Localization. *Diagnostics* **2022**, *12*, 1333. [CrossRef] [PubMed]

64. Sharma, S.; Ding, G.; Telikicherla, A.; Aghlmand, F.; Talkhooncheh, A.H.; Wang, M.; Shapiro, M.G.; Emami, A. 3D Surgical Alignment with 100 μm Resolution Using Magnetic-Field Gradient-Based Localization. In Proceedings of the 2020 IEEE International Solid-State Circuits Conference-(ISSCC), San Francisco, CA, USA, 16–20 February 2020; pp. 318–320.

65. Sharma, S.; Ramadi, K.B.; Poole, N.H.; Srinivasan, S.S.; Ishida, K.; Kuosmanen, J.; Jenkins, J.; Aghlmand, F.; Swift, M.B.; Shapiro, M.G.; et al. Location-aware ingestible microdevices for wireless monitoring of gastrointestinal dynamics. *Nat. Electron.* **2023**, *6*, 242–256. [CrossRef]

66. Northern Digital Inc. Aurora: Minimally Invasive Procedures with Electromagnetic Tracking Technology. Available online: https://www.ndigital.com/electromagnetic-tracking-technology/aurora/ (accessed on 2 April 2023).

67. Pholemus Tracking. Available online: https://polhemus.com/ (accessed on 29 March 2023).

68. Amfitrack. Next Generation Motion Tracking. Available online: https://www.amfitrack.com/ (accessed on 29 March 2023).

69. Paperno, E.; Plotkin, A. 3D magnetic tracking of a single subminiature coil with a large 2D-array of uniaxial transmitters. *IEEE Trans. Magn.* **2003**, *39*, 3295–3297. [CrossRef]

70. Plotkin, A.; Paperno, E.; Vasserman, G.; Segev, R. Magnetic tracking of eye motion in small, fast-moving animals. *IEEE Trans. Magn.* **2008**, *44*, 4492–4495. [CrossRef]

71. Plotkin, A.; Shafrir, O.; Paperno, E.; Kaplan, D.M. Magnetic eye tracking: A new approach employing a planar transmitter. *IEEE Trans. Biomed. Eng.* **2010**, *57*, 1209–1215. [CrossRef] [PubMed]

72. Islam, M.N.; Fleming, A.J. A novel and compatible sensing coil for a capsule in wireless capsule endoscopy for real time localization. *Proc. IEEE Sens.* **2014**, *2014*, 1607–1610. [CrossRef]

73. Yang, W.; Zhang, C.; Dai, H.; Hu, C.; Xia, X. A Novel Wireless 5-D Electromagnetic Tracking System Based on Nine-Channel Sinusoidal Signals. *IEEE/ASME Trans. Mechatron.* **2021**, *26*, 246–254. [CrossRef]

74. O'Donoghue, K.; Corvo, A.; Nardelli, P.; Shea, C.O.; Khan, K.A.; Kennedy, M.; Cantillon-Murphy, P. Evaluation of a novel tracking system in a breathing lung model. In Proceedings of the 2014 36th Annual International Conference of the IEEE Engineering in Medicine and Biology Society, Chicago, IL, USA, 26–30 August 2014; pp. 4046–4049. [CrossRef]

75. Islam, M.N.; Fleming, A.J. Resonance-Enhanced Coupling for Range Extension of Electromagnetic Tracking Systems. *IEEE Trans. Magn.* **2018**, *54*, 5700109. [CrossRef]

76. Nagaoka, T.; Uchiyama, A. Development of a small wireless position sensor for medical capsule devices. In Proceedings of the 26th Annual International Conference of the IEEE Engineering in Medicine and Biology Society, San Francisco, CA, USA, 1–5 September 2004; pp. 2137–2140. [CrossRef]

77. Jaeger, H.A.; Franz, A.M.; O'Donoghue, K.; Seitel, A.; Trauzettel, F.; Maier-Hein, L.; Cantillon-Murphy, P. Anser EMT: The first open-source electromagnetic tracking platform for image-guided interventions. *Int. J. Comput. Assist. Radiol. Surg.* **2017**, *12*, 1059–1067. [CrossRef]

78. O'Donoghue, K.; Eustace, D.; Griffiths, J.; O'Shea, M.; Power, T.; Mansfield, H.; Cantillon-Murphy, P. Catheter Position Tracking System Using Planar Magnetics and Closed Loop Current Control. *IEEE Trans. Magn.* **2014**, *50*, 5100209. [CrossRef]

79. Dai, H.; Song, S.; Zeng, X.; Su, S.; Lin, M.; Meng, M.Q.H. 6-D Electromagnetic Tracking Approach Using Uniaxial Transmitting Coil and Tri-Axial Magneto-Resistive Sensor. *IEEE Sens. J.* **2018**, *18*, 1178–1186. [CrossRef]

80. O'Donoghue, K.; Cantillon-Murphy, P. Planar Magnetic Shielding for Use With Electromagnetic Tracking Systems. *IEEE Trans. Magn.* **2015**, *51*, 8500112. [CrossRef]

81. O'Donoghue, K. *Electromagnetic Tracking and Steering for Catheter Navigation*; University College Cork: Cork, Ireland, 2014.

82. Vanden Berghen, F. Levnberg-Marquardt Algorithms vs. Trust Revion Algorithms. Available online: http://www.applied-mathematics.net/LMvsTR/LMvsTR.pdf (accessed on 30 March 2023).

83. Ortner, M.; Coliado Bandeira, L.G. Magpylib: A free Python package for magnetic field computation. *SoftwareX* **2020**, *11*, 100466. [CrossRef]

84. Chen, H.; Shyh-Liang Low, A. A Study of RF Power Attenuation in Bio-tissues. *J. Med. Biol. Eng.* **2004**, *24*, 141–146.

85. Sonntag, C.L.W.; Sprée, M.; Lomonova, E.A.; Duarte, J.L.; Vandenput, A.J.A. Accurate Magnetic Field Intensity Calculations for Contactless Energy Transfer Coils. In Proceedings of the 16th International Conference on the Computation of Electromagnetic Fields, Aachen, Germany, 25–28 June 2007; pp. 1–4.

86. Camelia, G. *Compilation of the Dielectric Properties of Body Tissues at RF and Microwave Frequencies*; King's College London: London, UK, 1996.

87. McCleskey, R.B. Electrical Conductivity of Electrolytes Found In Natural Waters from (5 to 90) °C. *J. Chem. Eng. Data* **2011**, *56*, 317–327. [CrossRef]

88. Castello-Palacios, S.; Valles-Lluch, A.; Garcia-Pardo, C.; Fornes-Leal, A.; Cardona, N. Formulas for easy-to-prepare tailored phantoms at 2.4 GHz ISM band. In Proceedings of the 2017 11th International Symposium on Medical Information and Communication Technology (ISMICT), Lisbon, Portugal, 6–8 February 2017; pp. 27–31.

89. Finite Element Method Magnetics. Available online: https://www.femm.info/wiki/HomePage (accessed on 29 March 2023).